UPPSALA
UNIVERSITET

Digital Comprehensive Summaries of Uppsala Dissertations from the Faculty of Science and Technology 441

Metal Oxide Thin Films and Nanostructures Made by ALD

MÅRTEN ROOTH

ACTA
UNIVERSITATIS
UPSALIENSIS
UPPSALA
2008

ISSN 1651-6214
ISBN 978-91-554-7220-7
urn:nbn:se:uu:diva-0

Dissertation presented at Uppsala University to be publicly examined in Å 2005, Ångströmlaboratoriet, Lägerhyddsvägen 1, Uppsala, Thursday, June 5, 2008 at 10:15 for the degree of Doctor of Philosophy. The examination will be conducted in Swedish.

Abstract
Rooth, M. 2008. Metal Oxide Thin Films and Nanostructures Made by ALD. Acta Universitatis Upsaliensis. *Digital Comprehensive Summaries of Uppsala Dissertations from the Faculty of Science and Technology*. 56 pp. Uppsala.

Thin films of cobalt oxide, iron oxide and niobium oxide, and nanostructured thin films of iron oxide, titanium oxide and multilayered iron oxide/titanium oxide have been deposited by Atomic Layer Deposition (ALD). The metal oxides were grown using the precursor combinations CoI_2/O_2, $Fe(Cp)_2/O_2$, NbI_5/O_2 and TiI_4/H_2O. The samples were analysed primarily with respect to phase content, morphology and growth characteristics.

Thin films deposited on Si (100) were found to be amorphous or polycrystalline, depending on deposition temperature and the oxide deposited; cobalt oxide was also deposited on MgO (100), where it was found to grow epitaxially with orientation $(001)[100]Co_3O_4||(001)[100]MgO$. As expected, the polycrystalline films were rougher than the amorphous or the epitaxial films. The deposition processes showed properties characteristic of self-limiting ALD growth; all processes were found to have a deposition temperature independent growth region. The deposited films contained zero or only small amounts of precursor residues.

The nanostructured films were grown using anodic aluminium oxide (AAO) or carbon nanosheets as templates. Nanotubes could be manufactured by depositing a thin film which covers the pore walls of the AAO template uniformly; free-standing nanotubes retaining the structure of the template could be fabricated by removing the template. Multilayered nanotubes could be obtained by depositing multiple layers of titanium dioxide and iron oxide in the pores of the AAO template. Carbon nanosheets were used to make titanium dioxide nanosheets with a conducting graphite backbone. The nucleation of the deposited titanium dioxide could be controlled by acid treatment of the carbon nanosheets.

Keywords: Atomic layer deposition, Metal oxide, Nanostructures, Template deposition, Thin films

Mårten Rooth, Department of Materials Chemistry, Box 538, Uppsala University, SE-75121 Uppsala, Sweden

ISSN 1651-6214
urn:nbn:se:uu:diva-0 (http://urn.kb.se/resolve?urn=urn:nbn:se:uu:diva-0)

List of papers

I **Atomic layer deposition of dielectric Nb_2O_5 films using the NbI_5-O_2 precursor combination**,
Mårten Rooth , Kaupo Kukli and Anders Hårsta, in EUROCVD 15, Proc. Vol. 2005-09, Eds.: A. Devi, R. Fischer, H. Parala, M. Allendorf and M. Hitchman (The Electrochem. Soc., Pennington, N. J. 2005) p. 598

II **Ordered and parallel niobium oxide nano-tubes fabricated using Atomic Layer Deposition in anodic alumina templates**,
Mårten Rooth, Anders Johansson, Mats Boman and Anders Hårsta, *Mater. Res. Soc. Symp.* 2006, 901E, 0901-Ra24-05.1

III A**tomic Layer Deposition of Co_3O_4 Thin Films Using a CoI_2/O_2 Precursor Combination**,
Mårten Rooth, Erik Lindahl and Anders Hårsta, Chemical Vapor Deposition, 2006, 12, 209

IV **Atomic layer deposition of iron oxide thin films and nanotubes using ferrocene and oxygen as precursors**,
Mårten Rooth, Anders Johansson, Kaupo Kukli, Jaan Aarik, Mats Boman and Anders Hårsta, Chemical Vapor Deposition 2008, 14, 67

V **ALD of titanium dioxide nanostructures using carbon nanosheets as a template**,
Mårten Rooth, Ronald A. Quinlan, Erika Widenkvist, Jun Lu, Helena Grennberg, Brian C. Holloway, Anders Hårsta and Ulf Jansson, submitted to Chemical Vapor Deposition

VI **Multilayered metal oxide nanotubes deposited in a template based process using atomic layer deposition**,
Mårten Rooth, Anders Johansson, Jun Lu, Mats Boman, Jan-Otto Carlsson and Anders Hårsta, in manuscript.

Comments on my own contribution to the papers in the thesis

I Major part of the planning. Major part of the experimental work. Major part of the writing.

II Half the planning. Half the experimental work. Half the writing.

III Major part of the planning. Half the experimental work. Major part of the writing.

IV Major part of the planning. Major part of the experimental work. Major part of the writing.

V Half the planning. Major part of the experimental work. Major part of the writing.

VI Major part of the planning. Major part of the experimental work. Major part of the writing

Contents

Abbreviations

AAO	Anodic Aluminium Oxide
ALD	Atomic Layer Deposition
CVD	Chemical Vapour Deposition
Cp	Cyclopentadienyl
EELS	Electron Energy Loss Spectroscopy
ERDA	Elastic Recoil Detection Analysis
GIXRD	Grazing Incidence X-Ray Diffraction
HRTEM	High Resolution Transmission Electron Microscopy
RBS	Rutherford Backscattering Spectroscopy
SEM	Scanning Electron Microscope
TEM	Transmission Electron Microscopy
XPS	X-ray Photoelectron Spectroscopy
XRD	X-Ray Diffraction
XRFS	X-Ray Fluorescence Spectroscopy

1. Introduction

Thin films and thin film structures in the nanometer range are objects of large interest with a wide variety of applications commonly found in everyday life. These structures can be found in computers, mobile phones, cars, solar cells, sensors of various types and numerous other components. What makes the objects in the nanometer range so interesting is that the physical properties found in nanostructures deviate from the properties known for microscopic objects of the same material [1]. The changes in physical properties can be associated with the high fraction of surface atoms in nanometer-sized objects. Decreased boiling point, shifting of the band gap and changes in the magnetic properties are known size effects [2-4]. Furthermore, the relatively large surface area of nanostructured thin films is also an effect of the increased surface to volume ratio of these structures. The changes in physical properties add an extra dimension to the field of materials science and can be used to tailor the properties of these minute structures but it can also lead to unwanted effects. Amongst the unwanted effects, tunnelling currents in metal oxide field-effect transistors [5] can be mentioned.

Thin films can be applied to surfaces to change the chemical and physical properties of a material. For example, thin films can be used to make a surface harder, reduce friction or chemical properties. Thin films can also be found in applications, such as gate oxides [5] or antireflective coatings [6]. Thin films having photo-catalytic properties can be used for photo-cleavage of water [7] or it can be used to keep a surface clean by decomposing organic particles[8]. Many of the applications put high demand on the thin film and often it has to be of a certain thickness or an excellent uniformity might be needed. A technique that can produce thin films which meet the high demands is atomic layer deposition (ALD)[9,10].

ALD, also known as atomic layer epitaxy (ALE) or atomic layer chemical vapour deposition (ALCVD), is a chemical gas phase deposition technique developed in Finland in the 1970´s by T. Suntola [9]. It should be mentioned that the ALD technique was also developed at roughly the same time in the former Soviet Union by the group of Aleskovskii [9].

In ALD the reactant gases are separately introduced to the substrates and growth is achieved through self-limiting surface reactions. This results in the high uniformity and an excellent thickness control for which the ALD technique is known, enabling deposition of very thin films with a uniform thickness [4]. The ALD technique is able to deposit a wide variety of compounds

such as oxides, nitrides and sulphides, as well as pure elements, mostly metals [9]. Furthermore, using the ALD technique, reactant species are enabled to reach into open cavities and evenly cover complicated structures. Closely related gas phase techniques like chemical vapour deposition (CVD) is usually unable to accomplish these types of depositions. The ability of the ALD technique to evenly cover complicated structures is of outmost importance when working with nanostructures [11].

One of the major challenges working with nanostructures is control of the size distribution. It is inherently difficult to make monodisperse nanostructures owing to coalescence of building blocks, continuous nucleation, growth and many other phenomena. One of very few nanostructured materials that come close to having a monodisperse size distribution is anodic aluminium oxide (AAO). AAO is a porous oxide with pore diameters in the nanoscale. Under certain conditions the pores formed can have a narrow size distribution (about 0.1%) with parallel pores in a close packed array [12]. Even though this structure fulfils the criteria of a narrow size distribution the material itself is not necessarily suitable for a certain applications. If another material is of interest there are several ways to transfer the pattern. One way is simply to cover the AAO membrane with a thin film of the desired material. The drawback with this method is that it is very difficult to deposit a conformal film covering the pore walls of the AAO membrane. However, one technique that is able to do this is ALD [11] and the ALD technique's ability to modify geometrically complicated surfaces, such as AAO membranes, is demonstrated in this thesis. Furthermore, the accurate thickness control of the ALD technique also makes an excellent tool for fine-tuning the pore diameters of the AAO membrane. The fine-tuning is of large interest since the pore diameters of AAO membranes are limited to certain intervals. By depositing a thin film of appropriate thickness in the AAO membrane, the gaps between the pore diameters possible to achieve by anodization of aluminium can be closed.

Free-standing nanotubes can be fabricated by depositing a thin film covering the pore walls of the AAO membrane. After deposition, the AAO membrane can be etched away to make free-standing nanotubes. The AAO membrane is easily etched away due to the poor chemical inertness of AAO. This results in nanotubes with a narrow size distribution, retaining the order of the template, which is also shown in this thesis. It is usually necessary to add a support for the nanotubes to prevent the structure from collapsing. This support can be a thin film or post-deposited rods inside the nanotubes.

The materials described in this thesis are thin films of niobium oxide, cobalt oxide and iron oxide. In addition, niobium oxide, iron oxide and titanium oxide has been deposited on structured substrates. Cobalt oxides are materials of considerable interest due to applications such as gas sensors [13], in electrocatalysis [14], as protective layers [15], in electrochromic devices [16,17], in solar-sensitive absorbers [18], and as electrode material

in thin-film supercapacitors (TFSC) [19]. Cobalt oxide also has possible applications in spintronics, where it is incorporated in a host matrix of a high bandgap metal oxide semiconductor [20–22]. Niobium oxide is a wide band gap dielectric material with a high index of refraction and has been reported to exhibit electrochromism [23]. These properties have made niobium oxide interesting for applications such as solar cells [24], oxygen gas sensors [25] and optical coatings [26] and as a dielectric layer [27]. Also iron oxide has many interesting properties and applications such as photo catalysis [28-30], sensors [31, 32] and interesting magnetic behaviour [33, 34]. Titanium oxide is a material with a high refractive index and high optical transparency over a wide spectral range. Titanium dioxide has a large commercial importance, with numerous applications and interesting properties such as biocompatibility [35], photo-catalysis [6-8] and solar cells [36].

2. Methods

In this chapter the different methods used for fabrication of thin films and nanotubes will be described. The chapter starts with a general description of the ALD technique for use in depositions on flat surfaces using a TiI_4/H_2O precursor combination for deposition of TiO_2 as an illustrative example. The following section describes deposition of thin films on structured surfaces using ALD. The chapter ends with descriptions of the anodization process of aluminium to make AAO membranes and of the preparation of carbon nanosheets..

2.1 Thin film deposition

ALD is a chemical gas phase deposition technique where reactant gas pulses are separately introduced to the substrates to be coated. Growth is achieved through self-terminating surface reactions [9]. Self-terminating mean that only one monolayer of reactant gas species can be adsorbed to the surface during a pulse. The pulses containing reactant gases are separated by purging pulses where the ALD reactor is flushed with an inert gas. The purging pulses ensure that the reactant gas pulses do not mix. Mixing of the reactant gas pulses would lead to continuous growth and an accurate thickness control of the deposition process would be lost. By-products like detached ligands and excess reactants are also flushed away by the purging pulses. A complete set of reactant gas pulses and purging pulses needed to deposit a certain compound are referred to as a cycle. If the deposition parameters have been chosen properly, the number of cycles rather then the concentration of the reactant species determines the film thickness. It should be mentioned that deviations from the ideal linear relation between the number of cycles used for deposition and the film thickness are not uncommon. There are two phenomena that account for these deviations, substrate enhanced growth [9] and substrate inhibited growth [9]. The different types of substrate related growth modes are illustrated in Figure 1. In the first case, with substrate enhanced growth, the growth per cycle (GPC) value is underestimated and the film is thicker than expected. In the other and more common case, with the substrate inhibited growth, the GPC is overestimated. The cause can be, for example, nucleation problems on the substrate but as soon as a coherent film has been deposited the process will have a linear relation

between the number of cycles used and the film thickness. In a case where the substrate does not affect the growth by either enhancing or inhibiting it, a strait line passing through the origin would be obtained (see figure 1).

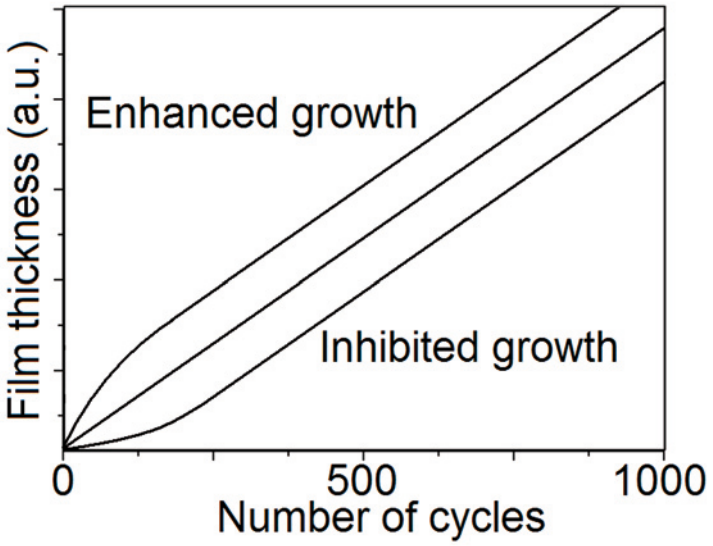

Figure 1. Schematic graph of the relation between the number of cycles and the film thickness and the influence the substrate can have if it enhances or inhibits the growth of the film deposited.

This thesis only discusses deposition of metal oxides. A major part of the thesis concerns deposition using metal halides or more specifically metal iodides as the metal precursor. Since the most frequently used precursor type is metal halides, the main part of the discussion will concern this precursor type. The other type of precursor used is an organometallic ALD precursor, ferrocene, which has good thermal stability and is also highly reactive. Organometallics are precursors where the metal is directly bonded to the carbon of the organic ligand. The other type of organic ALD precursors is the metalorganics, where the metal is not directly bonded to the carbon in the ligands; instead, the metal is bonded to the organic backbone of the ligand through oxygen, nitrogen or sulphur.

The metal halides are classified as being inorganic ALD precursors. The advantages with halide precursors are that they are small, reactive, thermally stable and usually leave small amounts of ligand residues in the deposited films. Small ligand reduces the risk for steric hindering and a resulting reduction of the GPC value. High thermal stability enables deposition without thermal decomposition at higher temperatures.

Many types of compounds have been deposited using metal halides such as oxides, nitrides, sulphides, fluorides and pure elements (see e. g. [9]). However, there are some drawbacks associated with the use of halide precursors in ALD. One is that HCl and HI are formed as by-products when water is used as the oxygen source. These by-products can etch the growing film leading to a reduced GPC value and poor film uniformity. Often this can be avoided by using O_2 as the oxygen source, but this is not always possible. Another drawback with halide precursors is that some metal halides have low vapour pressure and higher temperatures are needed for sufficient evaporation of the precursor. The evaporation temperature is the lowest temperature possible for deposition and even though a metal halide might be thermally stable the high evaporation temperature reduces the temperature interval where successful depositions can be achieved. Yet another but rather uncommon problem encountered in ALD processes, using metal halide precursors, is that the metal halide precursor adsorbed on the surface might react with the incoming oxygen precursor forming a volatile compound. One such example is the volatile oxychloride $NbOCl_3$, formed in the reaction between $NbCl_5$ and water [37].

As mentioned above many ALD processes using metal halide precursors leave low amounts of precursor residues in the film, but when using water as the oxygen source one should always be aware of the risk of hydrogen contamination in the deposited film. This problem can be solved by changing the oxygen source to e. g. O_2 or O_3. There are several oxygen sources available for use in ALD processes. In the experiments discussed in this thesis only water and oxygen has been used as oxygen sources but a few other worth mentioning are ozone (O_3), hydrogen peroxide (H_2O_2) and nitrous oxide (N_2O), see e. g. [9].

To deposit a metal oxide like TiO_2, four pulses are usually needed; two reactant gas pulses separated by two purging pulses. The first pulse in the TiI_4 / H_2O process is a TiI_4 pulse. The second and fourth pulses are purging pulses and the third pulse is a water pulse. During the first pulse TiI_4 is evaporated from a semi-open quartz boat, marked C in Figure 2.

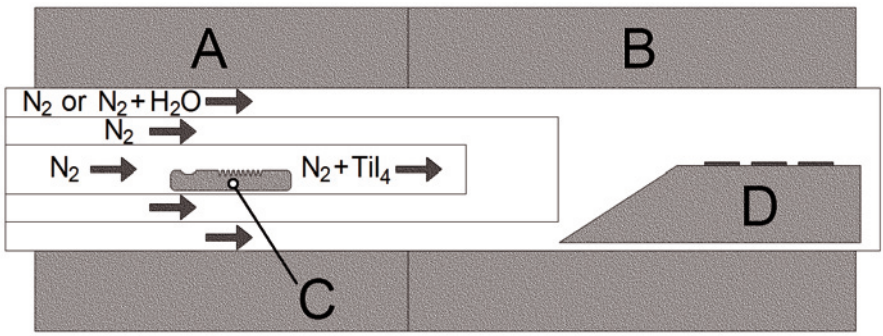

Figure 2. Schematic view of the ALD system.

The evaporated TiI_4 is carried with an inert gas from the evaporation zone, marked with an A in figure 2, to the substrates placed on the substrate holder (D) in the deposition zone (B). The TiI_4 adsorbs on the surface of the substrate by binding to the substrate surface, while at the same time loosing one or several iodide ligands. During the second pulse, the first of the two purging pulses, the detached iodide ligands as well as excess TiI_4 are flushed away. The iodide ligands are flushed away as I or I_2 in the absence of hydroxyl groups or water, with the ratio I/I_2 increasing with the temperature. Whenever hydroxyl groups or water are present, the main part of the iodide ligands will react with the hydroxyl groups or the water, forming HI to be transported away. With the titanium containing species adsorbed to the surface of the substrate and all excess precursor and by-products flushed away, water is introduced as a third pulse. Water will react with the adsorbed titanium iodide species to form HI and TiO_2. The last pulse in the cycle is the final purging pulse where HI and excess water is flushed away. The phase of the formed oxide film depends on the deposition temperature. In the example of TiO_2, rutile is formed at higher temperatures whereas anatase is formed at lower temperatures. Phase mixtures can also be deposited at intermediate temperatures. The absolute temperature where a transition between two phases occurs is in some cases strongly dependent on the substrate used for the deposition [38], but the film thickness can also influence which phase that is formed [38].

2.2 Deposition on structured substrates

Deposition on structured substrates e. g., substrates with structures having high aspect ratios, generally requires longer diffusion times and hence longer pulse lengths. Considering a pore with a diameter of a couple of tens of nanometers and a length of several microns; a gas phase molecule entering the pore opening, travelling down the pore will frequently collide with the pore wall. In fact, the molecule-wall collisions are a couple of orders of magnitude more frequent than molecule-molecule collisions in a pore of this size and with the pressures commonly used in ALD [39]. The molecule, travelling deeper into the pore, frequently colliding with the pore wall will sooner or later adsorb on an available adsorption site. In the case of a TiI_4 molecule, adsorption on the pore wall will result in the loss of one or more iodide ligands. The adsorbed titanium iodide species can now migrate along the surface further down the pore. Since lower metal iodides, i. e. metal iodides with fewer iodide ligands, have lower vapour pressure [40], the adsorbed titanium iodide species is not likely to enter the gas phase again unless it reacts with free iodide ligands to form TiI_4. The lower diffusion rate on the surface of the pore wall will increase the time needed to saturate the entire surface of the pores. Other factors increasing the time needed to saturate the

surface are the adsorption of iodide ligands, blocking adsorption sites [41] and the lower partial pressure of reactant species deeper inside the pores [42]. These factors result in the longer precursor pulses and purging pulses needed to successfully deposit conformal thin films on structured substrates.

Even though the discussion above has regarded deposition in pores, the same arguments apply for the opposite structure, i. e. arrays of nanotubes, nanosheets or nanorods aligned perpendicularly to the surface. If the distances between the nanostructures are much smaller than the mean free path, surface diffusion may have a significant contribution to the overall time to complete saturation of the surface.

2.3 Anodization of AAO

Aluminium is always covered by a thin native oxide layer, which protects the aluminium from further corrosion. The oxide layer can be made much thicker by anodization i.e. forced oxidation, thus providing better protection of the aluminium. The oxide formed during the anodization is porous, and by exposing the porous oxide to dyes, it is possible to trap the dyes in the pores, resulting in decorative colors. The actual trapping of the dye is made by immersion in boiling water or steam. Anodization of aluminium is a technique that has been used to increase durability as well as for aesthetic reasons for several decades. However, the pores formed in the oxide are usually not of the same size or parallel to each other. Techniques for anodization under more controlled conditions were developed in the 90's, in order to produce porous alumina with monodisperse pore diameters, ordered in a hexagonal pattern with the pores parallel to each other [36,43,44]. In the mid 90's, using a two step anodization process, Masuda et al.[36] produced AAO membranes with monodisperse pore diameters, parallel pores and the pores hexagonally ordered. A schematic image of such a structure can be seen in Figure 3.

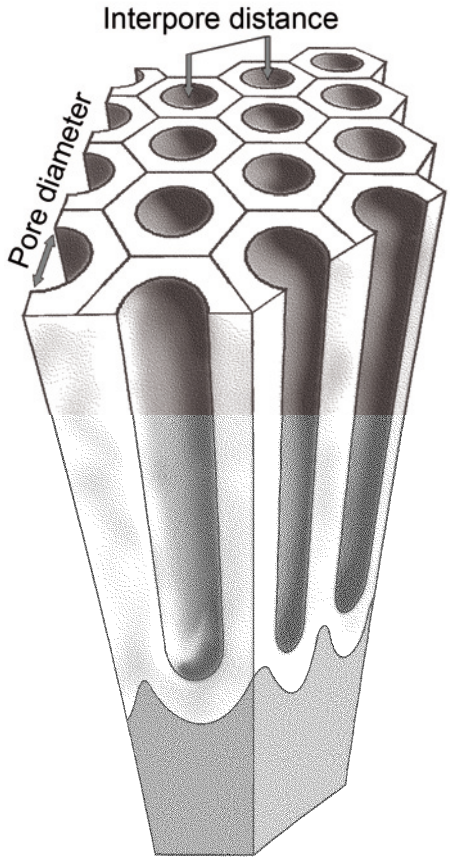

Figure 3. Schematic view of an AAO membrane.

By choosing the appropriate electrolyte and voltage, highly ordered and almost monodisperse arrays of pores, unique for the aluminium system, can be formed. In order to obtain hexagonally ordered porous alumina membranes it is necessary to anodize in an electrolyte which promote the dissolution of the formed alumina film [45].

Applying a constant voltage to an aluminium substrate, coupled as anode, an oxide layer rapidly starts to form. At first a continuous oxide layer is formed and this layer is usually referred to as the barrier layer. The oxide formation takes place at both the Al/Al_2O_3 interface due to the transport of O^{2-}/OH^- through the aluminium oxide film, and the Al_2O_3/electrolyte interface due to of migration of Al^{3+} outwards through the film [44]. Simultaneous with the oxide formation, a competing process occurs; the dissolvation of the formed oxide film. The dissolvation occurs by the electrolyte dissolving the aluminium oxide and the process is enhanced by the electric field over the oxide film. The electrical field is higher where the oxide film is

thin. A higher electric field promotes a more rapid dissolvation of the oxide, leading to formation of pores in the alumina film. The porous structure is created by the localized dissolvation of oxide in the pores and the formation of new oxide.

As mentioned earlier, a two-step process was used to produce AAO membranes with perfectly parallel pores, ordered in a hexagonal array [36]. During anodization the first pores formed are not ordered; rather they appear where the electric field initially is the strongest. As the anodization continues the pores start to order; the ordering occurs at the Al/Al_2O_3 interface leaving the parts of the pores near the Al_2O_3/electrolyte interface unordered. The ordering of the pores continues to improve for up to 18 hours, while longer anodization time does not improve the ordering of the formed oxide. Since the time to get a well-ordered oxide film is long it is important to keep the formation rate low in order not to consume too much aluminium. This can be achieved by performing the anodization at low temperatures, typically at 1 ºC. After reaching the point where the pores are ordered, the formed oxide film can be etched away, leaving an ordered array of hollows in the aluminium surface. Since the ordering of the pores occurs at the Al/Al_2O_3 interface, the array will be that of the ordered pores. If a subsequent anodization is performed, the array in the aluminium surface from the first anodization serves as pore initiation sites for the second anodization. The result is an oxide film with hexagonally ordered pores, parallel to each other with an almost monodisperse size distribution. The second anodization will also determine the thickness of the final AAO membrane, i. e. a long second anodization produces a thick membrane. After the second anodization the pore diameters can be tailored by immersion of the membrane in a solution which dissolve the oxide, e. g., phosphoric acid. By using different electrolytes and voltage during the anodization it is possible to control the inter-pore distance as well as the pore diameters [36, 43-45]. It might be mentioned that it is not possible to get ordered pores by applying an arbitrary voltage. Each electrolyte has a voltage regime where it is possible to produce AAO with ordered pores. A list of different electrolytes and for the electrolyte appropriate voltages can be found in Table 1.

Table 1. Anodization voltage and resulting inter-pore distances for different electrolytes.

Electrolyte	Inter-pore distance	Anodization voltage
Sulphuric acid (H_2SO_4)	~ 40 nm	25 V
Oxalic acid ($(COOH)_2$)	100 nm	40 V
Phosphoric acid (H_3PO_4)	420 nm	160 V

2.4 Preparation of carbon nanosheets

Carbon nanosheets are often referred to as graphene although the sheets in question are several nanometers thick, whilst true graphene only consists of a single graphite sheet. Carbon nanosheets consisting of several layers are structures of large interest. The sheets have superior electrical conductivity in the plane of the sheet and structures with surface areas exceeding 1000 m^2/g can be made [46]. The sheets can be deposited using radio frequency plasma enhanced chemical vapour deposition (RF-CVD) from a precursor mixture of ethane and hydrogen [47]. Using this method, sheets only a few atom layers thick and several microns in height and width can be made [47, 48]. A schematic image of a carbon nanosheet grown perpendicularly to the substrate can be seen in Figure 4. By applying an electric field during the deposition the sheets can be ordered relative to each other in the direction of the electric field [46].

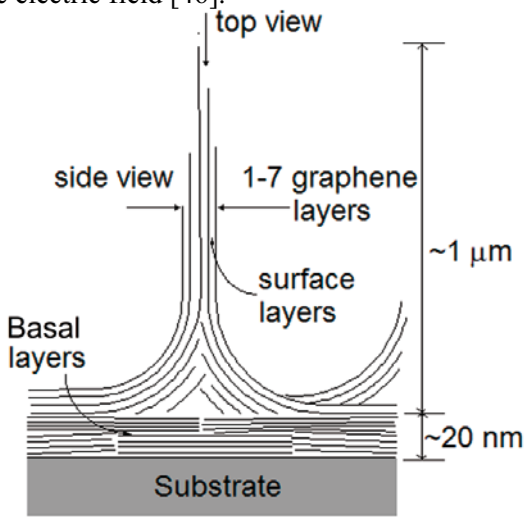

Figure 4. Schematic image of the carbon nanosheets structure.

The carbon nanosheets are ideal templates for the deposition of metal oxide nanosheets, except for one major drawback; the inert surface of the sp^2 hybridized carbon causes nucleation problems in an ALD process due to the lack of adsorption sites, making it difficult to deposit a continuous film without pinholes. A simple way to improve the nucleation is to treat the carbon nanosheets in hot hydrochloric acid solution prior to the ALD, although the activation of the surface can also be made using other methods [49]. During the acid treatment, holes are formed in the graphite sheets, the water present in the acid solution will react with the edges of the holes, resulting in holes that are terminated by OH and H groups [50]. The OH groups are good adsorption sites for the metal containing precursors and conformal thin

films can be deposited on the carbon nanosheets, resulting in metal oxide nanosheets with a conducting carbon backbone.

3. Experimental

In this chapter, the experimental parameters and the equipment used for synthesis are described. First, a description of the ALD reactor most frequently used in the experiments. This is followed by a general description of the deposition parameters and experimental set-ups for depositions on flat substrates like Si wafers. A section discussing deposition on structured substrates will follow; this section will also include the experimental parameters for the anodization of aluminium and the pre-treatment of carbon nanosheets. Post-treatment of samples, like the fabrication of freestanding nanotubes will also be found here. At the end of this chapter the different techniques used for characterization are described from an experimental point of view.

3.1 ALD

The ALD reactors used in the experiments are all hot-wall horizontal flow-type reactors. The reactors are basically constructed in the same way, and only the most frequently used reactor will be described in detail. A schematic view of the reactor can be found in Figure 2 in the introduction.

The reactor comprises of a 40 mm main quartz tube with two smaller quartz tubes, with diameters of 20 and 25 mm, respectively, arranged inside. The main tube is placed in a four zone furnace with gas inlets in one end and pressure control, a cold trap and a mechanical pump at the other end. The first two furnaces were used to evaporate the metal precursor from a semi-open quartz boat inserted in the innermost 20 mm tube. In Table 2 the vaporisation temperatures of the different precursors can be found. Nitrogen was used as carrier gas in the metal precursor pulse, t_1. To prevent diffusion of metal precursor to the deposition zone the pump was connected to the gas inlet side of the 20 mm tube, to provide a backflow during the purging and oxygen containing pulses.

Table 2. Vaporisation temperatures of the metal precursors.

Precursor	Vaporisation temperature
$Fe(Cp)_2$	55 °C
CoI_2	465 °C
NbI_5	320 °C
TiI_4	108 °C

During the purging pulses, t_2 and t_4, nitrogen was flushed through the main tube and the 25 mm tube. In the reaction pulse t_3, oxygen (99.998 %) or water was flowed into the main reactor tube, usually using a bulk flow of nitrogen. A constant bulk flow in the main reactor tube was used to keep the flow rate constant during all the pulses, t_1-t_4. The two last furnaces control the temperature of the deposition zone and in Table 3 the temperature intervals used for deposition as well as the total pressures are shown. Inside the deposition zone a TiN-coated titanium substrate holder was inserted at a desired distance from the orifices of the middle tube. The substrate holder can support five 12 mm × 12 mm substrates spread out longitudinally in the deposition zone and spaced by 10 mm gaps. Detailed descriptions of the two other reactors used can be found in Paper III and [51].

Table 3. Precursor combinations used for growth, deposition temperature and total pressure.

Material deposited	Precursor combination	Deposition temperature	Total pressure
Fe_2O_3/Fe_3O_4	$Fe(Cp)_2/O_2$	350-600 °C	10 Torr
Co_3O_4	CoI_2/O_2	475-700 °C	10 Torr
Nb_2O_5	NbI_5/O_2	350-600 °C	2 Torr
TiO_2	TiI_4/H_2O	200-300 °C	2 Torr

3.1.1 Flat substrates

Flat substrates, like wafers of Si (100), were frequently used to investigate the ALD characteristics of the different ALD processes. In the case of cobalt oxide depositions, MgO (100) substrates were also used to study epitaxial growth.

Prior to deposition the substrates were cleaned with ethanol in an ultrasonic bath, and in some studies the Si (100) samples were dipped in HF to etch away the native oxide. The GPC values at different pulse lengths were utilized to study the self-termination of the processes, keeping one of the four pulses constant whilst changing the fourth one. If the process is self-

terminating, the GPC value will increase when the length of the metal precursor pulse or oxygen precursor pulse is increased. As the pulse duration increases, the GPC value will gradually stop increasing and reach a steady state where it does not increase any more. If the precursor pulses behave in this way the process is most likely self-terminating. For the purging pulses the behaviour can be said to be the opposite. If the purging pulses are made longer the GPC value decreases until it reaches a steady value. Too short purging pulse may result in mixing of the precursors. If the growth continues the film thickness is not proportional to the number of cycles used but rather to the time used for deposition. One should bear in mind that the mixing of the precursor gas pulses caused by too short purging pulses can also lead to homogeneous nucleation in the gas phase. If this is the case significant amounts of the precursor may react before reaching the substrates, resulting in a lower GPC value or no growth at all. Series of experiments with different number of cycles used were made for the purpose of studying the relation between the number of cycles and the film thickness. The final characterisation of the ALD processes was made by a series of experiments performed at different temperatures. In this type of experiments the temperature window of the ALD process can be found. In the experiments determining the relation of the film thickness and the number of cycles and the GPC values at different temperatures, the pulse lengths found appropriate in the pulse length series described above were used.

3.1.2 Structured substrates

Two types of structured substrates have been used, AAO membranes and carbon nanosheets. As discussed in Chapter 2, longer pulses are needed for these substrates in order to deposit uniform films. Typically 30 seconds pulse durations were used to ensure complete separation of the precursor pulses and saturation of the substrate surfaces.

The AAO membranes used in this thesis were all in-house made, using oxalic acid as electrolyte. A schematic image of the anodization setup can be seen in Figure 4.

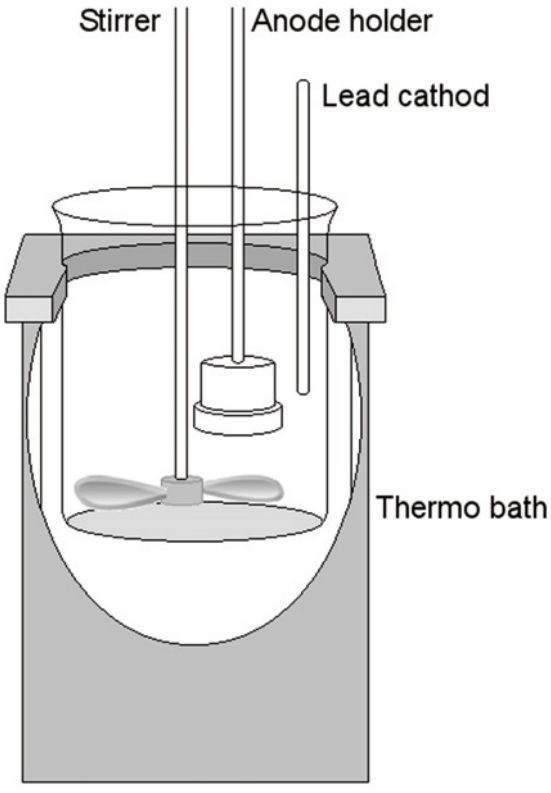

Figure 4. The experimental setup used for anodization of aluminium.

The membrane fabrication started with mechanically polished aluminium substrates from Goodfellow. The aluminium substrates were discs with diameters of 22 mm, thicknesses of approximately 0.5 mm and surface roughnesses of 1 Ra (arithmetic mean roughness) or better. The aluminium substrate was cleaned in 5 M sodium hydroxide, which effectively cleans the surface and forms a layer of aluminium hydroxide. The polished and cleaned substrate was electropolished in an electrolyte consisting of perchloric acid (65 %) and ethanol (99.5 %) with the volume ratio 1:4. A potential of 20 volt was applied and the substrate was polished for three minutes at a constant temperature of 1 ºC. After the electropolishing the aluminium substrate had a mirror like finish. The two subsequent anodizations were made in an oxalic acid electrolyte maintained at 1 ºC with an applied potential of 40 volt. The first anodization lasted for 18 to 20 hours to ensure good ordering of the pores at the oxide/aluminium interface. In order to fabricate AAO membranes, ordered from top to bottom, the oxide formed in the first anodization was etched away in a stripping solution. The stripping solution contained

chromic acid (1.8 wt-%) and phosphoric acid (6 wt-%). The pattern in the aluminium substrate from the first anodization acted as a template in the second anodization. The second anodization determined the thickness of the membrane and the oxide grew with a rate of 2 μm/hour. A schematic image of the two-step anodization process can be seen in Figure 5.

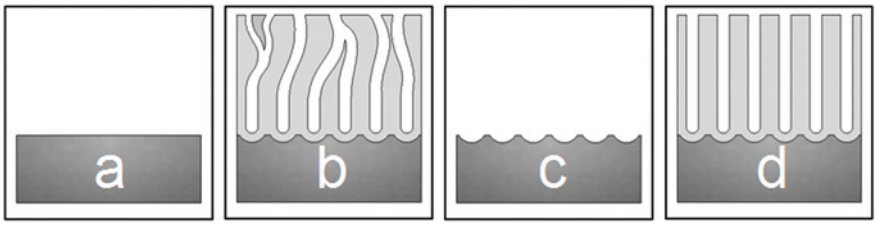

Figure 5. Schematic view of the two step anodization process. (a) The aluminium disc used for anodization. (b) The first anodization, the pores are ordered at the oxide/aluminium interface. (c) The removal of the oxide leaves the aluminium disk with shallow pits ordered in a hexagonal pattern. (d) The second anodization resulting in parallel and hexagonally ordered pores of the same diameter.

The pore diameter of the formed pores could be tailored by immersion in phosphoric acid (4.25 wt-%). 90 minutes of immersion in the given solution gave pores with a diameter of about 60-80 nm. However, it is difficult to control the pore diameter by carefully monitoring of the immersion time. This is probably due to different ageing of the formed oxide, but the process of ageing is not completely understood. Parameters that might influence the ageing process are the moisture of the air as well as the temperature and the quality of the chemicals used. It should be mentioned that the AAO membrane was not removed from the aluminium disk from which it was grown in the anodization. Since the aluminium disc was still present during the ALD experiments there was only one way open into the pore.

No other pre-treatment of the AAO membranes was made before the ALD experiments except for the pore-opening by immersion in phosphoric acid and the pre-heating initially made in the ALD experiments. The other type of structured substrate used, i. e. carbon nanosheets, were for the most part used as-received except for the pre-heating in the beginning of the ALD experiments. In some cases, the carbon nanosheets were acid-treated before the ALD experiments in order to improve the nucleation during the ALD. The acid treatment was made by immersion in hydrochloric acid, maintained at a temperature of 95 ºC for 6 hours.

3.1.3 Post treatment

Some of the AAO membranes coated using ALD were used to make free-standing nanotubes. It was possible to fabricate arrays of free-standing nano-

tubes, retaining the structure of the template by chemically removing the AAO membrane. However, it was necessary to add some support to be able to handle the substrates. Three different types of support were used; thin films made by CVD, silver rods deposited inside the metal oxide nanotubes using a wet chemical method and glue. A typical fabrication process is illustrated in figure 6; also included in the figure are scanning electron microscopy images of the different steps.

The supports were added to the structure after the ALD step but prior to the removal of the AAO membrane. In the case where a thin film deposited by CVD was used as support, the precursors used were the same as in ALD. The CVD support was made by switching the reactor to CVD mode, and the time of the deposition was 5 hours.

The silver rods used as support were made by the following wet chemical method. The ALD coated AAO membranes were immersed in a solution of silver nitrate ($AgNO_3$) with a concentration of 0.1 M. After the immersion the sample was heated to 500 ºC in air to thermally decompose the silver nitrate to silver, NO_2 and O_2. This process was repeated 10 times to make the supporting silver rods. The last type of support used was made by applying a layer of glue on the pore side of the AAO membrane.

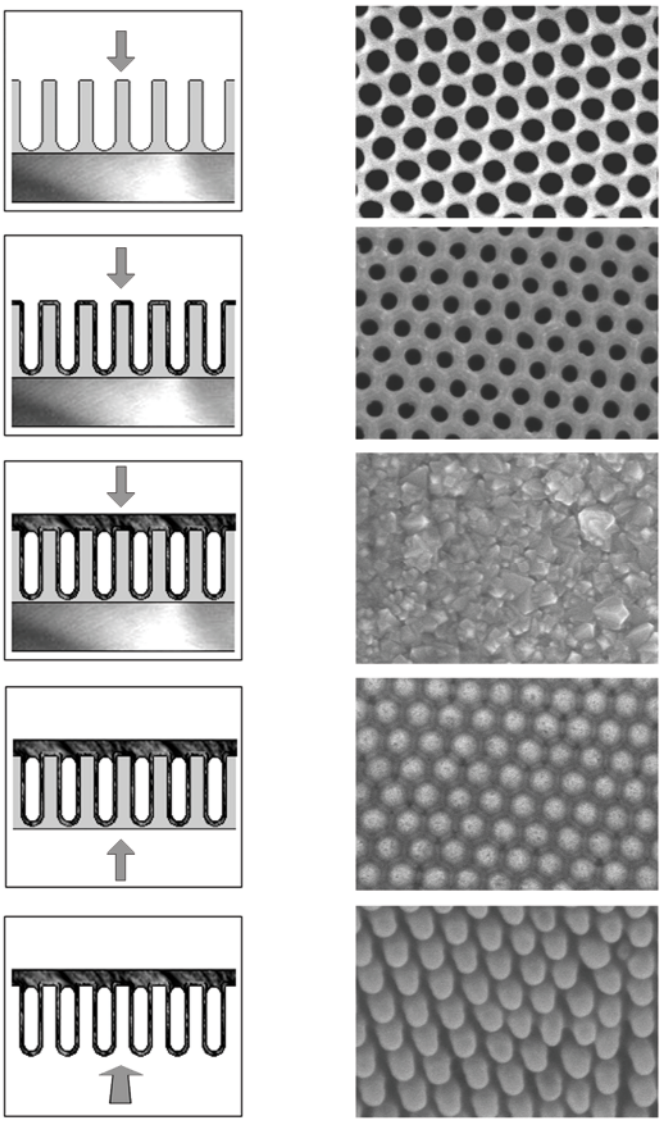

Figure 6. Schematic images and SEM images of the fabrication process where free-standing nanotubes were made. From the top, the AAO membrane; the second image, deposition of TiO_2. The third image; deposition of a thin film by CVD; the fourth image; removal of the aluminium disc by etching; the fifth image, the free-standing nanotubes. The arrow in the images to the left indicates from which direction the SEM image is taken.

In order to make the free-standing nanotubes the aluminium disc and the AAO membrane were removed. The aluminium was removed by etching in a solution of hydrochloric acid and copper chloride ($CuCl_2$). In this process copper is formed under a redox reaction in which aluminium is oxidized.

The AAO membrane was removed by etching in either phosphoric acid or sodium hydroxide. The choice of etching agent depended upon the metal oxide deposited. In the case of niobium oxide and titanium oxide phosphoric acid was used, but for iron oxide sodium hydroxide was used, since the phosphoric acid also dissolves the iron oxide.

3.2 Characterization

All SEM micrographs were made using a Leo 1550 instrument. Samples were mounted using carbon tape or in the case of cross section, on a specially made substrate holder where the samples could be pinned with the cross section facing the electron beam. Atomic force microscopy was also used to investigate the morphology of the samples and the analysis was made using a TopoMetrix TMX 2000 instrument.

A Tecnai F30ST (300 kV) instrument was used to make transmission electron microscopy (TEM) micrographs and electron energy loss spectroscopy (EELS) images of multilayered nanotubes and TiO_2 covered carbon nanosheets. The TEM images of Nb_2O_5 nanotubes were recorded using a JEOL 2000FXII (200 kV) instrument and also electron diffraction was made on this instrument. For the multilayered nanotubes, top view TEM specimens were prepared by grinding, polishing, dimpling and ion thinning from the back side of the sample. Finally the specimens were ion thinned from both sides in order to observe the interfaces between the layers. The TEM samples of TiO_2 covered carbon nanosheets did not need any preparation since the nanosheets were deposited directly on tungsten TEM grids. The Nb_2O_5 TEM samples were prepared by mechanically removing the nanotubes. The nanotubes were loosened using a spatula and ethanol to collect the nanotubes. The ethanol containing nanotubes was then applied to a TEM grid and the ethanol was left to evaporate leaving the nanotubes on the TEM grid.

X-ray diffraction (XRD) was made using two different diffractometers. X-ray reflectivity was made on a Siemens D5000 diffractometer and grazing incidence X-ray diffraction (GIXRD), θ–2θ scans, φ-scans and pole figures were made on a Philips X'pert diffractometer. In all measurements Cu Kα radiation was used. Raman spectroscopy was also used to determine the phase composition in the samples; the measurements were preformed on a Renishaw instrument using a 514 nm laser.

The relative amount of the different elements in the samples was measured using x-ray fluorescence spectroscopy (XRFS). The instrument used was a Spectrolab X2000 spectrometer. Contaminant elements heavier than sodium could also be detected using this technique.

X-ray photo electron spectroscopy (XPS) also known as electron spectroscopy for chemical analysis (ESCA) was primarily used to study the pos-

sible presence of contaminants in the samples. The technique also gives information about the oxidation state of the elements in the sample. The measurements were preformed on a Perkin-Elmer PHI 5500 multi-technique system.

Ion beam techniques were used to preform elemental depth profiles analysis, to find the stoichiometry of the samples and to detect residues from the precursor. The ion beam source was a tandem accelerator. Rutherford backscattering spectroscopy (RBS) using 2 MeV $^{4}He^{+}$ ions was used to detect precursor residues and other possible contaminants. Elastic recoil detection analysis (ERDA) was used to make elemental depth profiles analysis and to find the stoichiometry of the deposited compound using 44 MeV $^{127}I^{9+}$ ions.

The dielectric properties of the Nb_2O_5 films were measured after electron beam evaporation of aluminium electrodes through a shadow-mask with an effective electrode area of 0.204 mm^2. After film deposition, the backsides of the silicon substrates were etched in hydrofluoric acid and metallized by evaporating a 100-150 nm thick Al layer. The electrical measurements were carried out on Al/Nb2O5/p-Si(100)/Al capacitor structures. Capacitance-voltage (C-V) curves were recorded using a HP 4284A precision LCR-meter in a two-element series circuit mode. The stair-sweep voltage step was 0.05 V. The period between voltage steps was 0.5 s. The AC voltage applied to the capacitor was 0.05 V while the frequency of the AC signal was 500 kHz. The current-voltage (I-U) curves were measured with a Keithley 2400 Source Meter in the stair sweep voltage mode while the voltage step used was 0.02-0.05 V. Besides films in the as-deposited state, some samples were also annealed at 750 °C in O_2 for 20 min under atmospheric pressure. These samples were supplied with Al electrodes after the annealing procedure. All electrical measurements were carried out at room temperature.

4. Thin film growth

In this chapter results from growth experiments on flat substrates will be discussed. The type of flat substrates used were Si(100) and MgO(100). The materials deposited on the flat substrates were niobium oxide, cobalt oxide and iron oxide. The discussion will focus on the growth rates, phase compositions and morphologies.

4.1 Growth

The effect of the pulse duration in the ALD cycle was examined using series of depositions where the length of one of the pulses in the ALD cycle was changed while the other three were kept constant. In the CoI_2/O_2 and NbI_5/O_2 processes this was made by depositions on Si(100) substrates and the GPC values for the different pulse lengths were calculated from the film thickness after deposition. In the $Fe(Cp)_2/O_2$ process the relative GPC values were found using QCM and absolute values were found using cross section SEM micrographs from films deposited on Si(100). In Figure 7, the effect of the length of the metal precursor pulses on the GPC values are shown. It can be seen that the iodide containing precursors saturates after about 4 s and the ferrocene precursor after about 2 s.

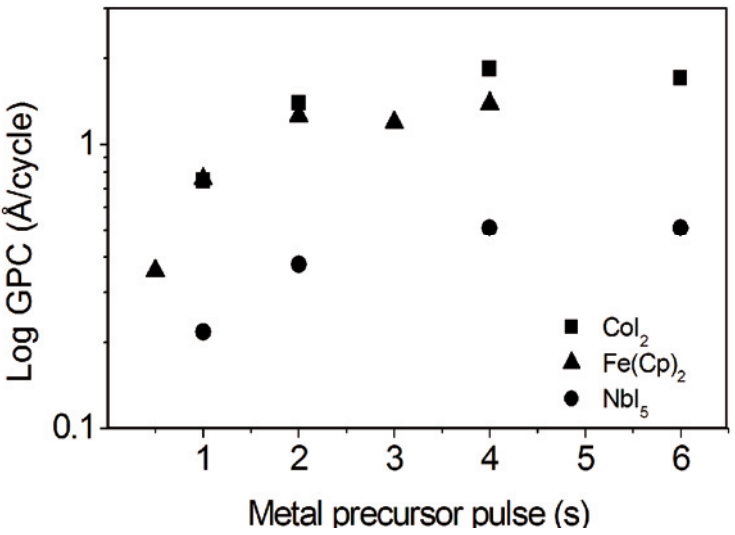

Figure 7. The influence of the length of the metal precursor pulse on the GPC value. Note the logarithmic GPC scale.

The deposition temperatures used in these experiments were 525 °C for the deposition of Co_3O_4 and 350 °C for the deposition of Fe_2O_3/Fe_3O_4 and Nb_2O_5. Even though the depositions were made in different reactors, the reactors are fairly similar. The linear gas flow velocity was about 0.5 to 1 m/s and the distance between the precursor and the substrates were about 0.5 m. The gas transport of the precursor should then be completed in 1 s. In the case of the $Fe(Cp)_2/O_2$ process, QCM was used to study the effect of pulse duration in the ALD cycle. In this study Fe_2O_3/Fe_3O_4 was grown on Fe_2O_3/Fe_3O_4 so any substrate related nucleation problems would not affect the growth rate. In the case of the other two processes the growth starts on Si(100) substrates. When comparing metal precursor pulse lengths, t_1, for these three processes, the iodide containing precursors appear to need somewhat longer time for saturation of the substrate.

The effect of the O_2 pulse duration in the ALD cycle was also examined in the same way and the results are shown in Figure 8. It can be seen that the O_2 pulse saturates after about 3-4 s for the metal iodide processes while the O_2 pulse in the ferrocene process saturates after about 7 s.

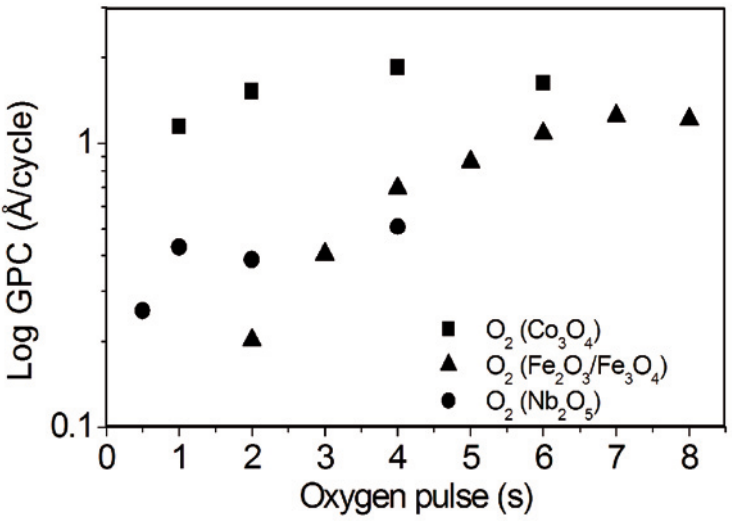

Figure 8. The influence of the length of the O_2 precursor pulse on the GPC value. Please note the logarithmic GPC scale.

In contrast to the metal precursor pulse series, the $Fe(Cp)_2/O_2$ process takes the longest time to saturate in the O_2 pulse series. The $Fe(Cp)_2$ and the NbI_5 pulse series are made at the same deposition temperature. The shorter O_2 pulse length needed for the NbI_5 process is most likely connected to the reactivity of the precursor towards oxygen and the time needed for the O_2 pulse to saturate in the ferrocene process could probably be lowered by increasing the deposition temperature. In the QCM study this was not possible due to the temperature instability of the QCM crystal.

The temperature dependence was also investigated for the three processes (see Figure 9). The studies were made using different temperature intervals due to the different vaporisation temperatures of the metal precursors, see Table 3 in Chapter 3.

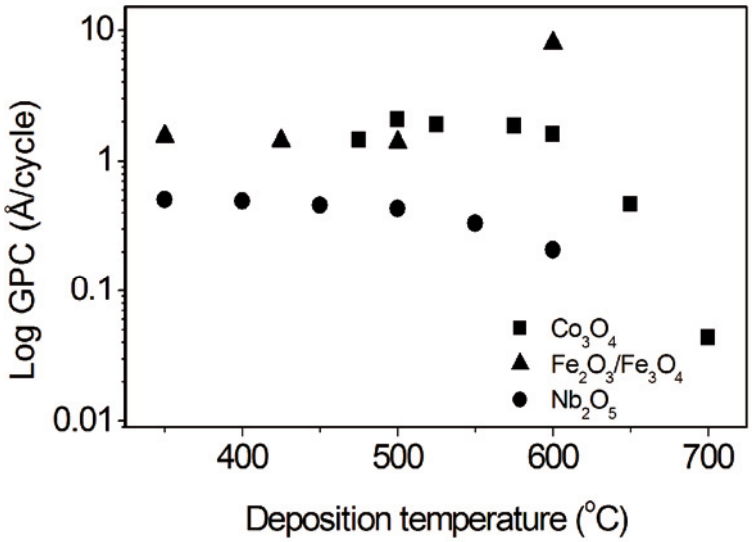

Figure 9. GPC values of the metal oxides at different deposition temperatures.

The Fe_2O_3/Fe_3O_4 and the Co_3O_4 processes had GPC values of about 0.15-0.2 nm/cycle in the temperature independent region while the Nb_2O_5 process had a lower GPC value of about 0.5 nm/cycle or lower as the temperature increased. One explanation to the observed GPC values can be the size of the adsorbed metal species, although many other factors also affect the growth rate. On an arbitrary surface it should be possible to pack the same amount of the two precursors of equal size but fewer of a larger precursor. This would theoretically result in higher GPC values for a process with the smaller ligands. The size of I^- and Cp is roughly the same and it was found experimentally that the GPC values of the Fe_2O_3/Fe_3O_4 and the Co_3O_4 processes were roughly the same. If the NbI_5 molecule looses less than four iodide ligands as it adsorbs on the surface, the size of the adsorbed species should be considerably larger than that of the adsorbed species of the other two precursors. The size of the adsorbed species NbI_x species could thus be an explanation for the lower GPC values observed in the Nb_2O_5 process.

Another difference is the temperature dependence of the processes at higher temperatures. The GPC value decreases as the temperature increases for both the metal iodide precursors while the ferrocene precursor has the opposite behaviour. The reason for the increasing GPC values, in the case of the Fe_2O_3/Fe_3O_4 process is decomposition of the ferrocene precursor. In the case of the metal iodides the decreasing growth rate can be explained by desorption of adsorbed species.

Co_3O_4 was also deposited on MgO(100) substrates. The same deposition parameters were used as for the depositions on Si(100). The temperature

dependence was also investigated for the growth on MgO(100). It was found that the GPC values were lower on MgO(100) substrates (0.08-1 nm/cycle) as can be seen in figure 10.

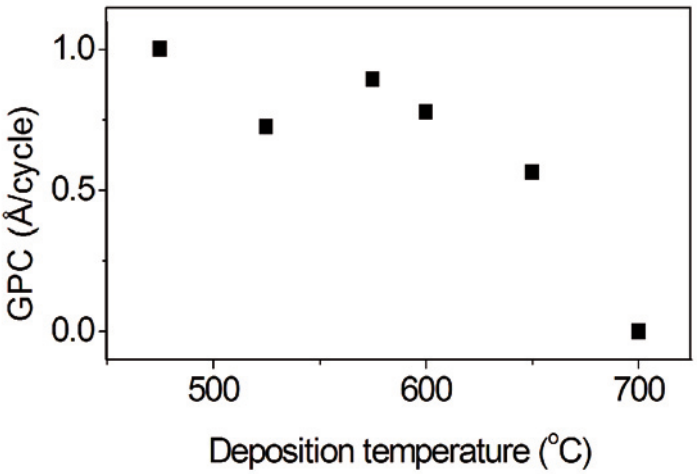

Figure 10. GPC values of Co_3O_4 deposited on MgO(001) substrates.

4.2 Film purity

In the metal iodide processes no iodine or other contaminants could be found in the films using XRFS. Also RBS measurement on a Co_3O_4 film deposited at 475 °C gave the same result. The detection limit for the two methods is below 0.1% for RBS and below 1% for XRFS. It can be mentioned that in the depth profile made using ERDA of the Co_3O_4 film deposited at 575 °C small amounts of carbon was found at the surface of the film. This carbon probably originates from the ambient atmosphere. The possible presence of contaminants in the Fe_2O_3/Fe_3O_4 films was examined using XPS. It was found that the carbon content in the films decreased with increasing deposition temperature, being the highest at 350 °C, with a carbon content of 3 at.%. For deposition temperatures of 425 °C and above, the carbon content was about 1 at.%. After sputter cleaning of the surface, no variation in the carbon content could be seen upon depth profiling of the deposited films. No other contaminants were found in any of the deposited films. However, most likely the films also contain hydrogen, but the presence of hydrogen can not be detected by XPS.

4.3 Electrical characterization

The results of the capacitance-voltage measurements imply that although the dielectric losses in the Al/Nb_2O_5/Si structures were noticeable (dissipation factor 0.5-0.8); the C-V curves tended to accumulate at negative biases already in the as-deposited state. The flat-band voltage was at around -0.3 V, shifting after O_2 annealing towards -0.8-(-1) V. Annealing at 750 °C in O_2 was carried out in order to decrease the amount of oxygen vacancies and reduce the related defect density; the annealing successfully reduced the interface trap state density and brought dramatic improvement to the film resistivity. However, a side-effect of the annealing was a reduction of accumulation capacitance. The capacitance equivalent oxide thicknesses (CET) values were 3.3 nm and 2.8 nm for as-deposited 34 nm and 25 nm thick Nb_2O_5 films; in the annealed dielectrics, the respective CET values increased to 4.3 nm and 4.7 nm. A more detailed discussion of the results of the electrical characterisation can be found in Paper I.

4.4 Phase composition

The phase composition of the deposited films was examined using XRD. Polycrystalline films were analyzed using GIXRD and θ-2θ scans. Pole figures, φ-scans and θ-2θ scans were used for textured films. All films deposited were crystalline except for the Nb_2O_5 films that were found to be amorphous at low temperatures. This is in agreement with earlier studies made with ethoxide precursors using ALD on glass substrate [52] and CVD [53], where amorphous Nb_2O_5 films have been reported to form below 450 ºC. At higher temperatures, 450 °C and above, crystalline films were deposited. All peaks in the diffractogram at 450 °C can be identified as belonging to orthorhombic Nb_2O_5. When the deposition temperature was increased, peaks from hexagonal Nb_2O_5 start to appear and were dominating at 600 °C as can be seen in Figure 11.

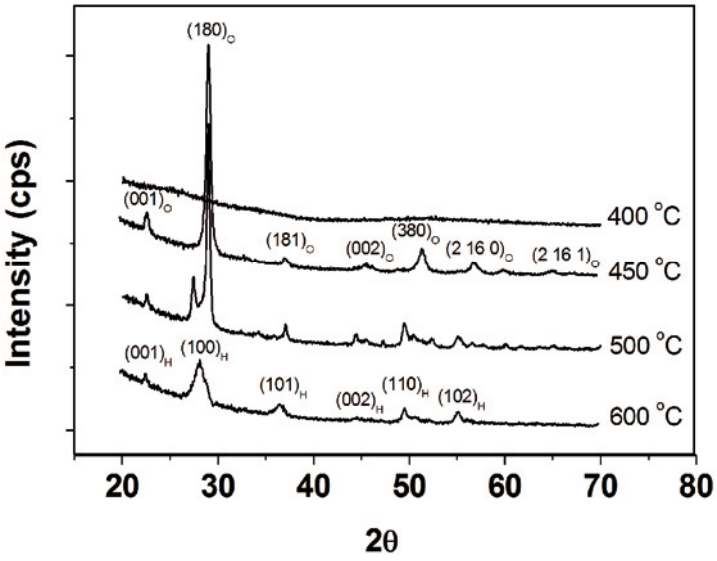

Figure 11. Diffractograms of Nb_2O_5 films deposited at different temperatures. The subscripts O and H denote the orthorhombic and hexagonal Nb_2O_5 phases, respectively.

Co_3O_4 films were deposited on both Si(100) and MgO(100) substrates. The XRD analysis showed that the films grown on Si(100) were polycrystalline and consisted of the cubic Co_3O_4 phase throughout the temperature interval 475–650 °C (Figure 12). No diffraction peaks from other phases in the Co-O system (e. g., CoO) were observed. Furthermore, the films grew without any preferred orientation, since the intensities of the reflexions agreed fairly well with those for a texture free sample [54]. From 475 to 650 °C, films deposited on MgO(100) were found to grow with a pronounced [400] orientation and only the 400 and 800 reflections of Co_3O_4 can be seen in the θ-2θ scan, as exemplified by the insert in Figure 12.

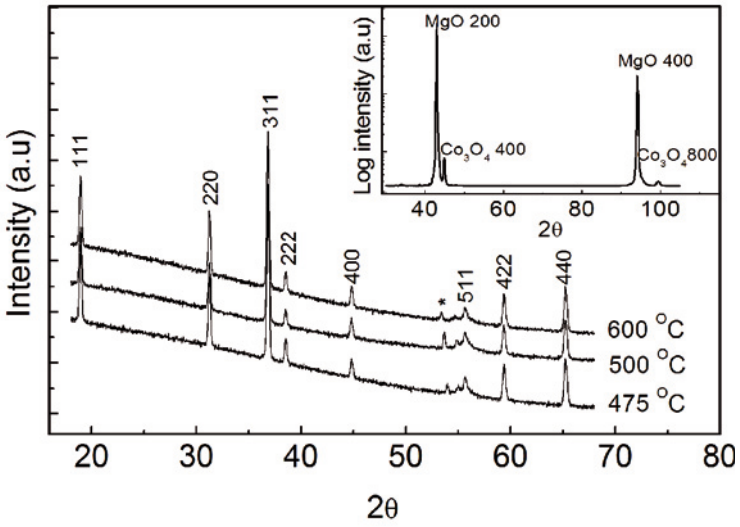

Figure 12. GIXRD patterns for Co_3O_4 films deposited on Si(100). The peak marked with an asterisk originates from the substrate. The insert is a θ-2θ scan of a sample deposited on MgO (100) at 475 ºC.

For films deposited on MgO(100), φ-scans (not shown here) were recorded to determine the orientational relation between the film and the substrate. For all deposition temperatures, the Co_3O_4 films were found to have the same orientational relationship to the MgO(001) substrate. The in-plane orientation was determined to be (001)[100]Co_3O_4 ||(001)[100] MgO, i.e., cube on cube.

The in-plane directional lattice mismatch, defined as $(d_{film}-d_{substrate})/d_{substrate}$ was found to be -4.04 %. Twice the value of the MgO lattice dimension (a = 4.21 Å) was used in the calculations since the unit-cell dimension of Co_3O_4 (a = 8.08 Å) is roughly twice as large as the corresponding MgO value. In Figure 13, the {044} pole of Co_3O_4 can be seen for a film deposited at 600 °C using 1000 deposition cycles. It can be mentioned that all pole figures recorded for films deposited from 475 to 600 °C were similar. As can be seen in Figure 13, no other orientations than those corresponding to the reflections of the symmetry equivalent {044} planes can be observed. This means that the films have been growing with one specific relation to the MgO(100) substrate. Furthermore, no twinning is present, indicating good epitaxial quality.

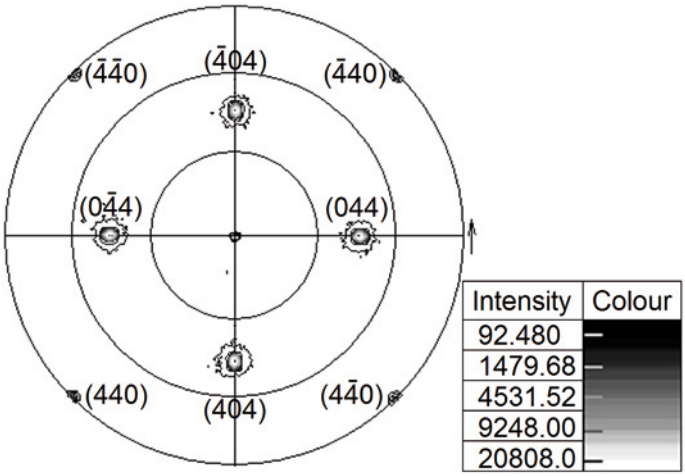

Figure 53. {044}-pole figure of a film deposited on MgO(001) at 600 ºC.

The stoichiometry of a film deposited on MgO(100) at 575 °C was also investigated using ERDA. It was found the the stoichiometry throughout the film corresponded to that of Co_3O_4 as can be seen in Figure 14.

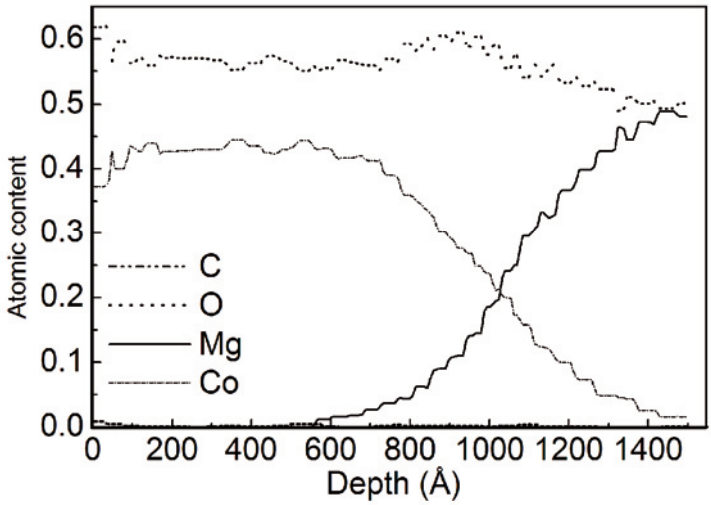

Figure14. Depth profile elemental analysis made with ERDA of a sample deposited on a MgO (100) substrate at 575 °C using 1000 cycles. The stoichiometry coincides with that of Co_3O_4.

Iron oxide films deposited on Si (100) in the temperature range of 350 to 600 °C and GIXRD showed that all samples were crystalline (Figure 15). Although the thicknesses of the samples deposited at 350 – 500 °C were of

the same magnitude. The diffraction pattern of the sample deposited at the lowest temperature had weaker peaks indicating that the film might be partially amorphous. Only hematite, the rhombohedral phase of Fe_2O_3, could be found in samples deposited at 500 °C and above. At temperatures below 500 °C another phase was present as well. The reflections belonging to the second phase were in agreement with the diffraction patterns of both magnetite (Fe_3O_4) and maghemite (Fe_2O_3). The two possible alternatives are both cubic with similar cell parameters. Although only magnetite has a close packed lattice, the reflections from planes containing both odd and even indices in maghemite are very weak. Since these reflections could not be seen in any of the diffraction patterns, it was not possible to distinguish between the two phases. If any of these reflections had been observed, the second phase could have been identified as maghemite. In contrast, the absence of these reflections does not necessarily imply that magnetite is present. The XRD data does thus not provide enough information to unambiguously identify the second phase. Attempts to identify the unknown phase using XPS failed, probably due to preferential sputtering.

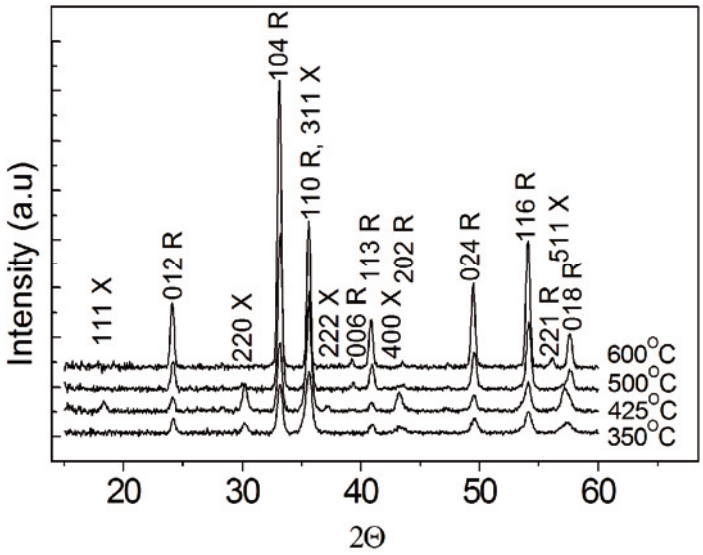

Figure 15. GIXRD patterns of iron oxide films, R denotes rombohedral and X denotes the unknown phase.

4.5 Morphology

In Figure 16, SEM images of Co_3O_4 films deposited on Si(100) are shown. It can be seen that the crystallite size increased as the temperature increased. The crystallites also appear to have sharper edges at lower temperatures.

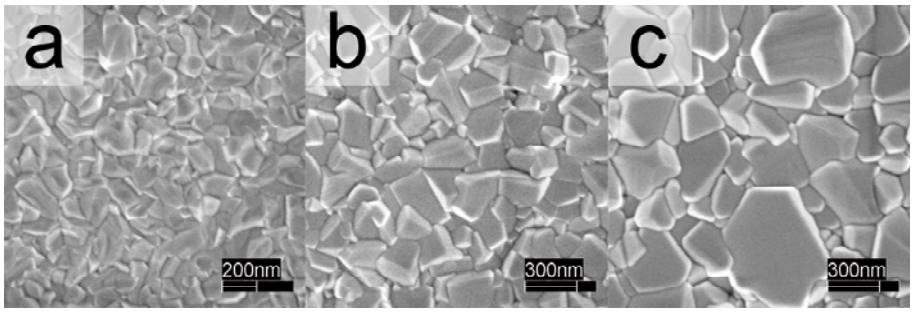

Figure 16. SEM images of Co_3O_4 deposited at, a) 500 °C, b) 550 °C and c) 600 °C. All three films were deposited using 1000 cycles.

The Co_3O_4 films deposited on MgO(100) substrates were much smoother than the ones deposited on Si(100). As mentioned above the films deposited on MgO(100) substrates grew with a pronounced [400] orientation. AFM images of samples deposited on MgO(100) can be seen in Figure 17. In the image of the sample deposited 600 °C square shaped structures ordered relative to each other can be seen, which can be an affect of the orientation of the film.

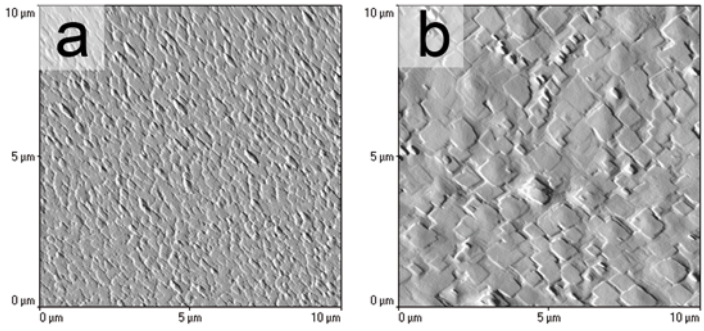

Figure 17. AFM images of Co_3O_4 deposited on MgO(100) substrates at, a) 475 °C and b) 600 °C. Both films were deposited using 1000 cycles.

The iron oxide samples all had similar appearances in the SEM images. The films were rough as can be seen in the SEM image in Figure 18.

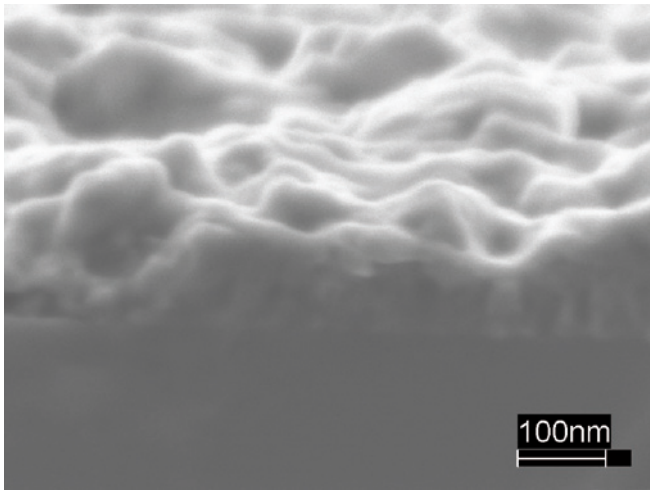

Figure 18. SEM image of Fe_2O_3/Fe_3O_4 deposited at 425 °C on Si(100).

The niobium oxide deposited at lower temperatures resulted in amorphous films that were smooth. Crystallites started to appear at 400 °C in the film as can be seen in the SEM image (Figure 19) but no peaks were seen in XRD. At higher temperatures crystallites could be clearly seen in the SEM images.

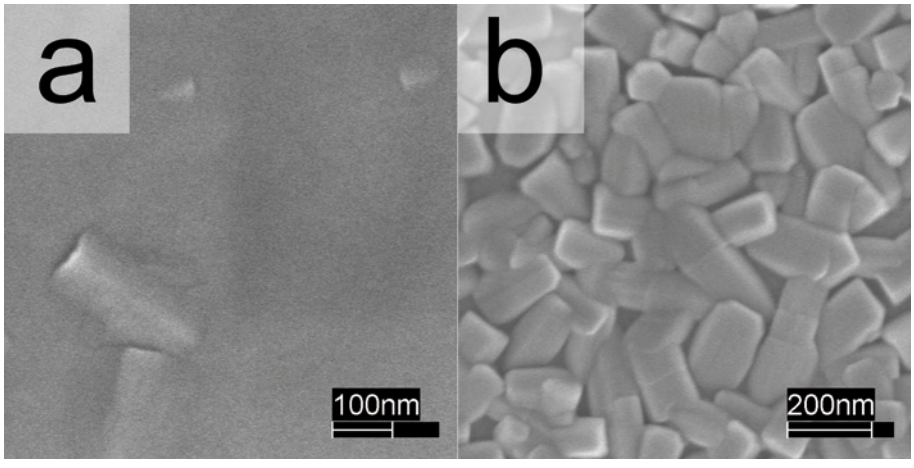

Figure 19. SEM images of Nb_2O_5 deposited at a 400 °C and b 525°C.

5. Nanostructured films

In this chapter nanostructured films will be discussed. The nanostructured films were made using templates, and two types of templates were used, AAO membranes and carbon nanosheets. Nanotubes were fabricated using AAO membranes as templates. The templates were covered with a thin film deposited by ALD. The thin films deposited were Nb_2O_5, Fe_2O_3/Fe_3O_4 and multilayered TiO_2-Fe_2O_3/Fe_3O_4. The Nb_2O_5 nanotubes were amorphous while all other nanotubes were crystalline, except for the TiO_2 layer deposited at 200°C in the multilayer nanotubes. In some cases, the template was etched away to make free standing nanotubes. Carbon nanosheets were covered with TiO_2 to make oxide nanosheets. No post-treatment was preformed on the nanosheets but some of the sheets were acid treated to improve nucleation before ALD was performed.

5.1 Nb_2O_5 nanotubes

Nb_2O_5 was deposited in AAO membranes using the precursor combination NbI_5/O_2. The AAO membranes used as templates all had inter-pore distances of 100 nm, pore lengths of 2 μm and pore diameters of 40 to 80 nm. The diameter and length gives the pores aspect ratios of 50 to 25. The AAO membranes used were only open in one end as can be seen in figure 6 in chapter 3. The deposited nanotubes retained the structure of the template even after the AAO membrane was etched away. It was also possible to tailor the diameters of the nanotubes by using AAO membranes with different pore diameters as can be seen in Figure 20.

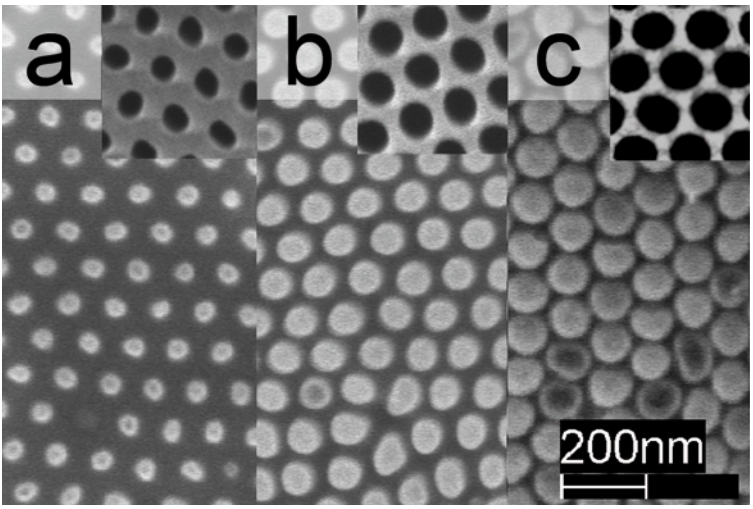

Figure 20. SEM images of Nb_2O_5 nanotubes and AAO membranes. The diameter of the AAO membranes used are, a) 40 nm, b) 60 nm and c) 80 nm.

In order to prevent the nanotubes from collapsing, a thin film was deposited on the pore side of the sample using CVD. The supporting film was grown from the same precursor combination that was used in the ALD process to deposit the nanotubes. By removing the AAO membrane in H_3PO_4 it was possible to make free standing nanotubes that were attached to a thin film as can be seen in figure 21.

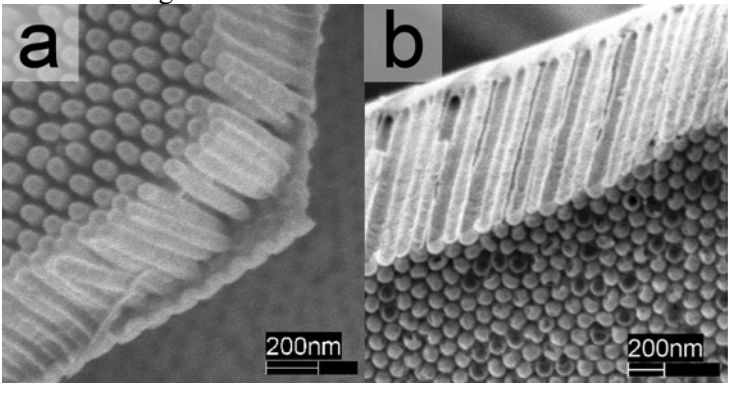

Figure 21. SEM images of free standing nanotubes of Nb_2O_5 supported by a thin film of the same material. The pore diameters of the nanotubes are 60 nm in a) and 80 nm in b).

The nanotubes were grown using 150 cycles at a deposition temperature of 400 °C. The resulting wall thickness was about 5 nm, i.e. with a GPC value of 0.03 nm/cycle. This GPC value was lower than the GPC values on flat Si(100) substrates. Using the same precursor combination and the same

deposition temperature it has been found that the growth rate on Si(100) is just below 0.05 nm/cycle (see Paper I). Different substrates can result in different GPC values, but the lower growth rate might also be a result of a lower partial pressure of O_2 in the pores. The effect of the O_2 partial pressure on the growth rate is known in ALD of metal oxides [42]. Another reason for the lower GPC values can of course also be desorption of adsorbed species during the long purging pulses.

The phase content of the deposited nanotubes was determined using electron diffraction. It was found that the nanotubes were amorphous. This agrees with the results from deposition on flat substrates at 400 °C, where the films formed also were amorphous. No traces of precursor residues could be found using XRFS.

5.2 Fe_2O_3/Fe_3O_4 and multilayer nanotubes

Fe_2O_3/Fe_3O_4 nanotubes and multilayered nanotubes were fabricated using AAO membranes as templates. The same precursor combination $Fe(Cp)_2/O_2$, that was used on flat substrates was used in the fabrication of the Fe_2O_3/Fe_3O_4 nanotubes. The Fe_2O_3/Fe_3O_4 nanotubes were deposited at 400 °C while the iron oxide in the multilayered nanotubes was deposited at both 400 and 500 °C. The multilayered nanotubes were fabricated by deposition of Fe_2O_3/Fe_3O_4 and TiO_2. The TiO_2 was deposited at 200 and 300 °C using TiI_4 and H_2O.

Free standing nanotubes of Fe_2O_3/Fe_3O_4 were made by removing the AAO membrane used as template. The AAO template was removed using NaOH since, as mentioned earlier, H_3PO_4 not only dissolved the AAO but also the Fe_2O_3/Fe_3O_4 nanotubes. In Figure 22, Fe_2O_3/Fe_3O_4 nanotubes can be seen prior to and after the AAO membrane was etched away.

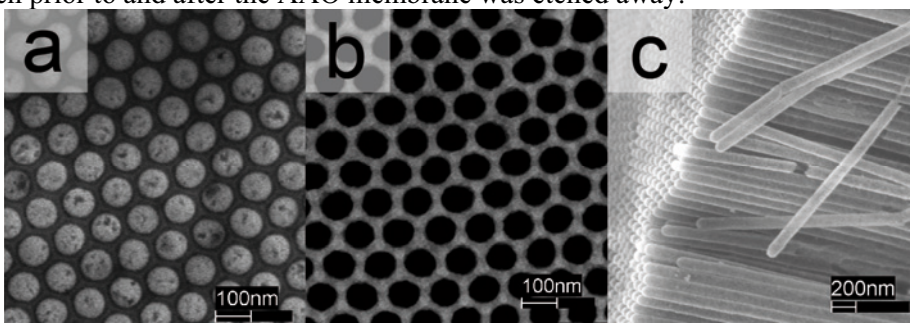

Figure 22. SEM images of Fe_2O_3/Fe_3O_4 nanotubes deposited using AAO membrane as a template. In a the Al disc has been removed and the tip of the nanotubes can be seen in the AAO matrix. In b the pore side can be seen and in c the free standing nanotubes can be seen.

For the samples where the AAO membrane was etched away, the Fe_2O_3/Fe_3O_4 nanotubes were supported by either glue or silver rods. The glue was applied on the pore side prior to the removal of the template. The silver rods were also deposited prior to the removal of the template. The silver rods were deposited by a wet chemical process where the samples were immersed in a solution of $AgNO_3$ and after that heated to 500 °C. It is not clear to which extent the nanotubes were filled with silver, but it was enough to function as a support. A SEM image of a sample where the free standing nanotubes are supported by silver rods can be seen in Figure 23.

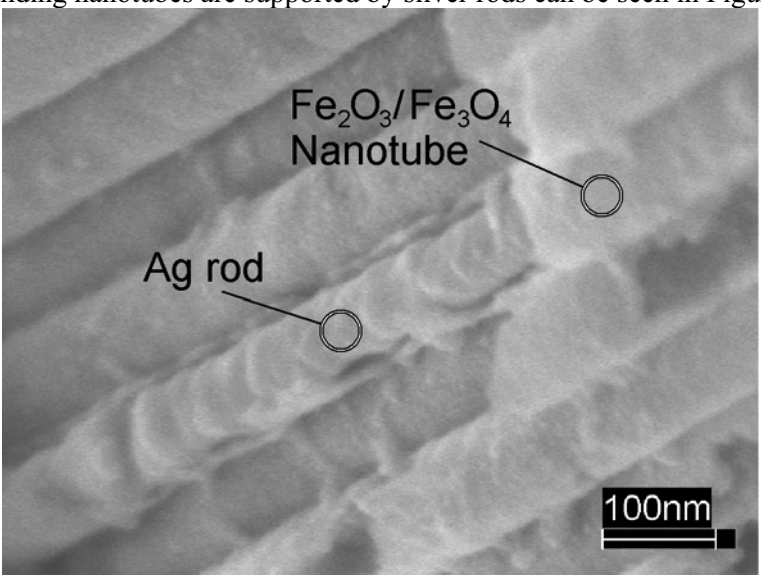

Figure 23. SEM image of free standing Fe_2O_3/Fe_3O_4 nanotubes supported by silver rods. One of the silver rods can be seen where the nanotubes have been damaged.

The GPC values of the Fe_2O_3/Fe_3O_4 nanotubes deposited at 400 °C were determined to be 0.06 nm/cycle. This is lower compared to the corresponding GPC values on flat Si (100) substrates which was 0.14 nm/cycle. A reduced growth rate inside the pores also observed in for the Nb_2O_5 system (see Paper II).

The AAO membrane was not etched away in the case of multilayered nanotubes. The multilayered nanotubes were fabricated by depositing three layers of two different metal oxides (titanium dioxide and iron oxide) on the pore walls of the AAO template by ALD. The precursor combinations used were TiI_4/H_2O and $Fe(Cp)_2/O_2$. The first layer was a TiO_2 film deposited at 300 °C using 200 ALD cycles, the second layer was iron oxide deposited at 400 or 500 °C using 50 ALD cycles and the third and final layer was again TiO_2 but this time deposited at 200 °C using 50 ALD cycles. The reason for choosing a different deposition temperature for this layer was to demonstrate the possibility to control the phase content in addition to the type of material.

A HRTEM image of the three layered structure is shown in Figure 24. It can be seen that the second TiO_2 layer is amorphous, while the other two layers are crystalline.

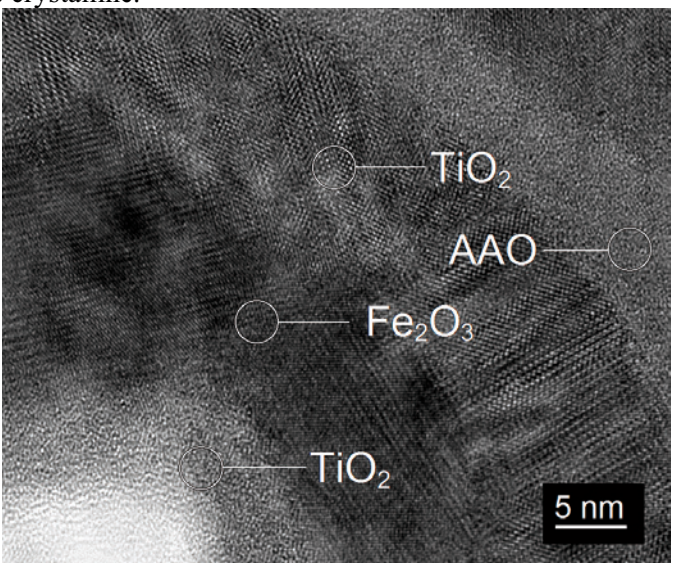

Figure 24. HRTEM image of the three layers.

EELS maps of a section of the resulting multilayer structure can be seen in Figure 25, where the layers of TiO_2, Fe_2O_3 and TiO_2 as well as the AAO matrix can be seen. The mapping was acquired using the Ti M 2,3 peak in Figure 25 a and Fe M 2,3 in Figure 25 b.

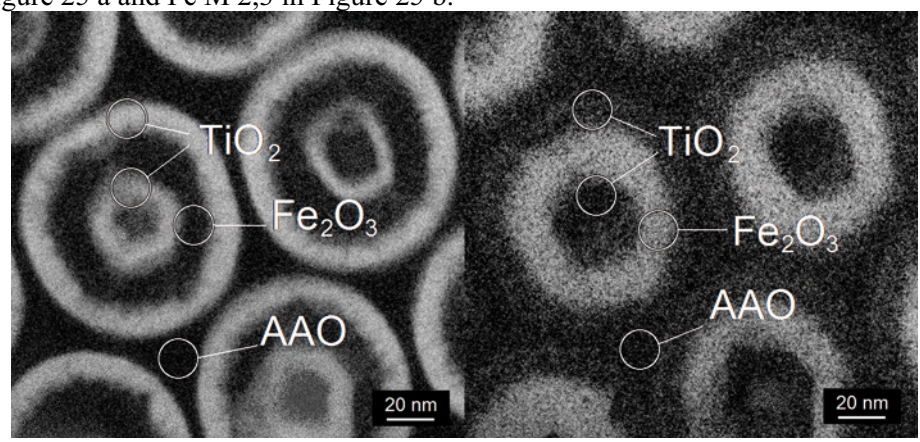

Figure 25. EELS map of multilayered nanotubes. In a the contrast of Ti is enhanced and in b the intensity of Fe is enhanced.

The GPC value of the iron oxide, deposited on top of the TiO_2 inside the pores was found to be 0.16 nm/cycle at 500 °C. A possible explanation to the

higher GPC values of Fe_2O_3 observed for the multilayer nanotubes depositions at 500 °C compared to the singlelayer iron oxide nanotubes deposited at 400 °C can be a contribution to the growth from thermal decomposition, since the depositions were made at a higher temperature in this study. From the ALD study of iron oxide described earlier it was observed that the GPC value increased by roughly 500 % when going from 500 to 600 °C due to thermal decomposition of the ferrocene precursor, whereas no increase could be seen between 400 °C and 500 °C [IV, 55]. However, the deposition experiments in that study was made on flat substrates employing much shorter pulse lengths (2 s), where possible slight thermal decomposition would not be noticeable. In contrast, the long pulse lengths (30 s) used in the present study would yield more time for thermal decomposition to occur. Another possible contribution to the high GPC value observed might be that the previously deposited TiO_2 layer favours the growth of the iron oxide. The GPC value of the TiO_2 layer deposited in the pores of the AAO was found to be about 0.06 nm/cycle. The corresponding GPC value of titanium dioxide deposited on flat substrates (Si 100) using the same process parameters is about 0.12 nm/cycle [56]. As in the other studies made using AAO as a template it is found that the GPC value is lower when depositing in pores compared to deposition on flat substrates.

The phase composition of the iron oxide nanotubes was the same as on Si(100) substrates. The Fe_2O_3/Fe_3O_4 nanotubes had a phase mixture of hematite and the not unambiguously identified phase, magnetite or maghemite. In the study of multilayered nanotubes two bi-layered samples were prepared. These samples were prepared in the same way as the multilayered nanotubes but without the last TiO_2 layer. The bi-layered samples were used to study the influence of the iron oxide deposition temperature on both the phase content of iron oxide and the effect on the phase content of the initially deposited TiO_2. In these samples, TiO_2 was deposited at 300 °C using 200 cycles and was subsequently covered with iron oxide deposited at either 400 °C or 500 °C using 50 cycles. After deposition of iron oxide, the only difference between the two deposition temperatures is the intensity ratio of the peaks at 35.6° and 33.2° in 2θ (see right insert in Figure 25). It can be seen that for the film deposited at 400 ºC this ratio is higher than for the film deposited at 500 ºC. Since the hematite phase has reflections at both these 2θ values while magnetite/maghemite only has a reflection at 35.6°, this observation indicated that the iron oxide deposited at 400 °C consisted of the phase mixture mentioned above while at 500 °C the nanotubes consisted of hematite (Figure 26).

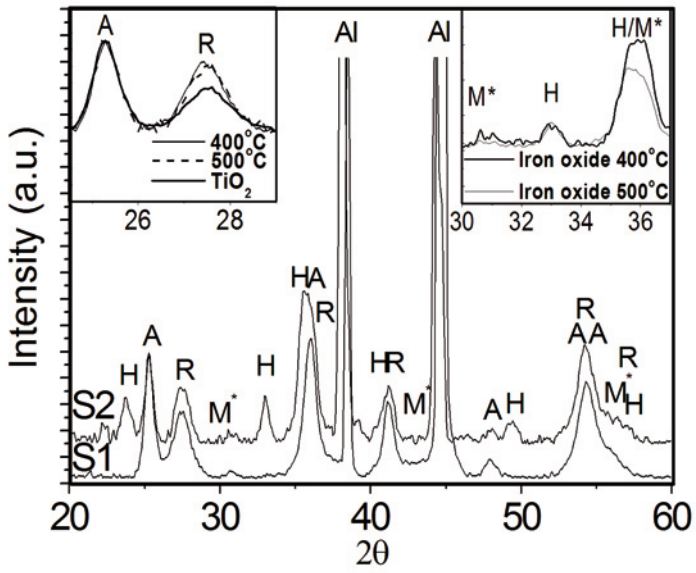

Figure 26. GIXRD patterns of samples with TiO_2 (S1) and TiO_2/Fe_2O_3 (S2) deposited in AAO membranes (H=hematite, M=magnetite/maghemite, R=rutile and A=anatase). The left insert shows the intensities of the rutile 110 and anatase 101 reflections before and after iron oxide deposition at two different temperatures and the right insert shows the intensities of two iron oxide reflections, where iron oxide was deposited at two different temperatures.*

The pure TiO_2 films consisted of a mixture of rutile and anatase as can be seen in Figure 26. After iron oxide deposition both TiO_2 phases were still present. The intensity of the rutile 110 reflection increased after the iron oxide deposition (figure 25 and left insert). This was observed for both deposition temperatures of the iron oxide, and is probably connected to an annealing effect of TiO_2 during the iron oxide deposition. However, earlier studies have indicated that the phase transformation of anatase to rutile does not occur at temperatures as low as the ones used for the iron oxide deposition [57, 58]. These studies were made on phase pure anatase samples, while the samples in this study are phase mixtures of anatase and rutile. The phase transition could thus be catalysed by the rutile crystallites present in the initial sample.

5.3 TiO_2 nanosheets

TiO_2 nanosheets were made using carbon nanosheets as templates and depositing a thin film of TiO_2 on the sheets using ALD. The sheets were typi-

cally ~ 1 µm high and were formed on top of a ~ 20 nm thick graphite-like film. The surface area of the sheets was about 1000 m^2/g [46]. The TiO_2 was deposited using the TiI_4/H_2O precursor combination at a deposition temperature of 300 °C. The films were deposited using 50 to 100 cycles. Depositions were made on as received carbon nanosheets and on acid treated nanosheets. Coleman et. al. have demonstrated that an acid-treatment of the carbon nanosheets with HCl induces defects in the graphene structure [50] and such defects can thus be favourable adsorption sites for precursor molecules.

Continuous films could not be obtained using less than 100 cycles on as received carbon nanosheets. Films deposited with 50 or 75 cycles consisted of separated crystallites. Even though the films deposited using 100 cycles were continuous, pinholes in the film could be seen in the TEM images. SEM and TEM images of samples deposited on as received carbon nanosheets can be seen in Figure 27.

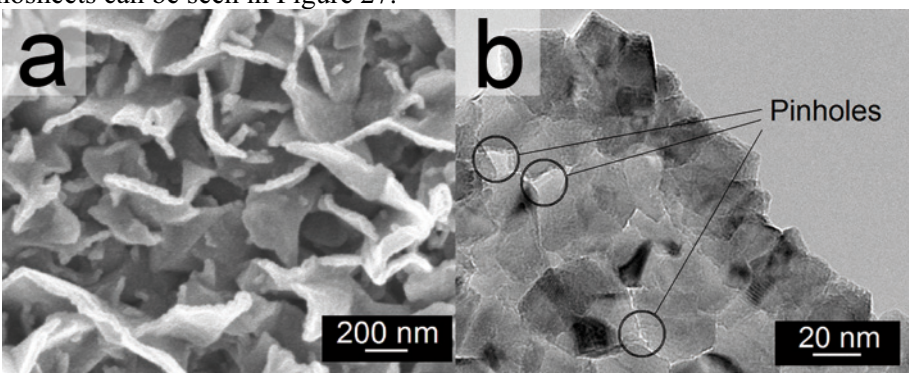

Figure 27. a) SEM image of a titanium dioxide film deposited on as-received carbon nano sheets on W substrate at 300 °C using 100 ALD cycles. The carbon nanosheets are viewed from the top. b) TEM image of a sample with carbon nanosheets grown on a tungsten TEM grid, the TiO_2 was deposited using the same deposition parameters as the sample in the SEM image. The single carbon nanosheet is viewed from the side. Pinholes are highlighted in the TEM image.

The reason for the poor nucleation might be the lack of adsorption sites, defects, on the inert surface of sp^2 hybridized carbon. Nucleation problems have earlier been observed for depositions on single walled carbon nanotubes [49]. Depositions were thus made on acid treated carbon nanosheets to investigate if the nucleation could be improved. As can be seen in Figure 28, the nucleation was considerably improved by the acid treatment and a more or less continuous film of titanium dioxide is obtained after only 50 ALD cycles.

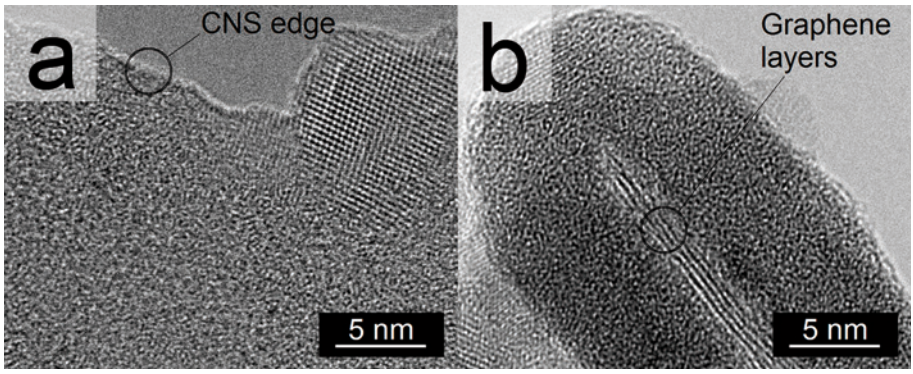

Figure 28. TEM image of acid-treated CNS deposited with 50 ALD cycles of TiO_2 at 300 °C. a: Sample viewed from the side perpendicular to the graphene planes. b: Sample viewed from the side showing the graphene layers of a carbon nanosheets.

X-ray diffraction (XRD) analysis showed that titanium oxide films on both the as-received and acid-treated carbon nanoshets contained the anatase phase of TiO_2 (see Figure 29). XRD measurements on samples deposited with only 50 ALD cycles did not show any crystalline peaks, which can be explained by the small crystallite sizes as well as the small amount of material deposited. No rutile reflections could be found in any of the deposited films. This agrees with an earlier ALD study using the same precursor combination and a deposition temperature of 300 °C, where anatase was also deposited.[56]

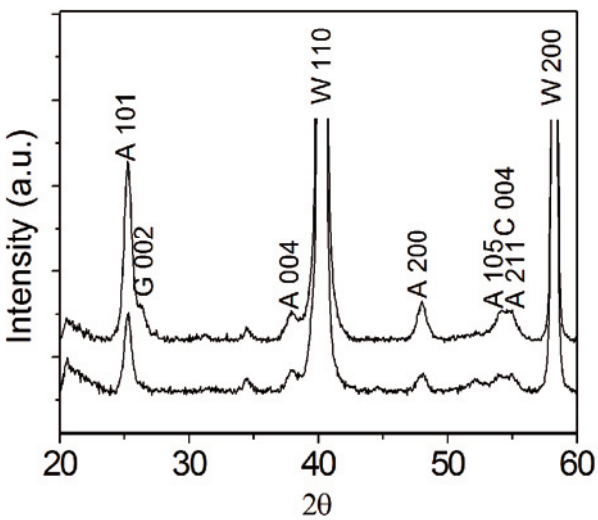

Figure 29. X-ray diffractogram of samples deposited with 100 ALD cycles on acid-treated carbon nanosheets and non acid treated carbon nanosheets. Peaks attributed to anatase, nanosheets and tungsten are marked with A, G and W, respectively.

The Raman analysis confirmed that anatase was present in all the deposited films with the well known bands of anatase observed at 147, 404, 521 and 635 cm-1 [59]. Typical Raman spectra of samples deposited on both acid-treated and as-received carbon nanosheets can be seen in Figure 30. The samples were deposited under the same conditions, using 50 ALD cycles while the sample in the spectrum in the insert in Figure 30 was deposited using 100 cycles. The intensity was higher on the acid-treated samples since more material was deposited on this substrate.

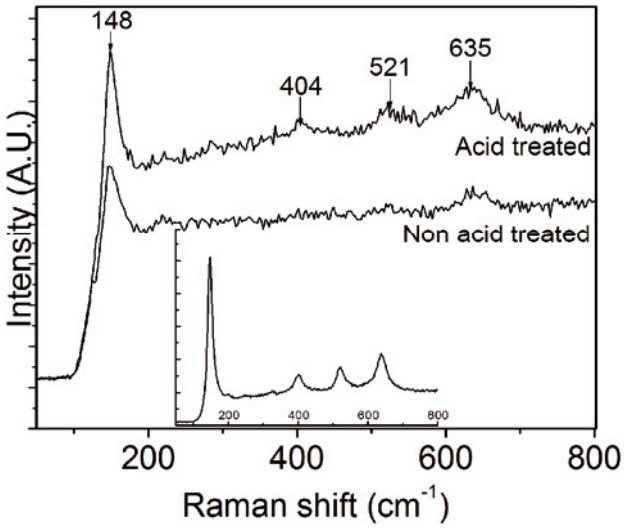

Figure 30. Raman spectra of TiO_2 deposited on acid-treated and as-received carbon nanosheets using 50 ALD cycles. The insert shows a Raman spectrum of an acid-treated sample deposited using 100 ALD cycles.

6. Concluding remarks

In this thesis it has been demonstrated that thin films of Co_3O_4, Fe_2O_3/Fe_3O_4 and Nb_2O_5 can be deposited using ALD from the precursor combinations CoI_2/O_2, $Fe(Cp)_2/O_2$ and NbI_5/O_2. The processes showed ALD characteristics with self-limiting growth. The deposited films were uniform, but the surface roughness was high in some cases.

Co_3O_4 and Fe_2O_3/Fe_3O_4 films were found to be crystalline at all temperatures, although the Fe_2O_3/Fe_3O_4 films might be partially amorphous at lower temperatures. The Fe_2O_3/Fe_3O_4 crystallised as a phase mixture of hematite and a not unambiguously identified phase below 500 °C; above this temperature phase pure hematite was deposited. The Co_3O_4 crystallised as the cubic Co_3O_4 phase at all deposition temperatures examined. Co_3O_4 was also deposited on MgO(001) substrates where it was found to grow epitaxially in the [400] direction, with the in plane orientation (001)[100]Co_3O_4 ||(001)[100] MgO, i.e., cube on cube. Nb_2O_5 deposited at 400 °C or below was amorphous; above this temperature the films grown were crystalline. The films crystallised in the orthorhombic phase at 450 °C, while at 500 °C peaks belonging to the hexagonal phase could also be seen and at 600 °C only the hexagonal phase was observed.

The films had low contamination levels and for films deposited using metal iodide precursors no contaminants could be found. In the Fe_2O_3/Fe_3O_4 films deposited using $Fe(Cp)_2$ as Fe precursor, low levels of carbon could be found. However, the Fe_2O_3/Fe_3O_4 films might also contain hydrogen, not detectable by the analysis techniques used.

The use of AAO membranes as templates for nanotube fabrication has also been demonstrated. AAO membranes with monodisperse pore diameters, parallel pores and the pores hexagonally ordered can be grown using a two step anodization process. The nanotubes were fabricated by depositing a thin film covering the pore walls of the AAO. Nb_2O_5 and Fe_2O_3/Fe_3O_4 nanotubes were grown using the same precursor combinations as were used on the flat substrates. The nanotubes had a uniform wall thickness and nanotubes with aspect ratios, of up to 50, were deposited. Thin film deposition can be used to fine-tune the pore diameter at the same time as it improves the properties of the AAO, e. g. chemical inertness. The AAO can also be etched away to make free standing nanotubes, where the nanotubes retain the structure of the template, but to achieve this, a support has to be added on the

backside. The supports used were thin films grown by CVD, silver rods deposited using a wet chemical method and glue.

Multilayered nanotubes were also fabricated using AAO as a template. The multilayer structure was made by depositing Fe_2O_3/Fe_3O_4 at 400-500 °C and TiO_2 at 200-300 °C. The nanotubes consisted of the phase mixture of Fe_2O_3/Fe_3O_4 mentioned above, rutile, anatase and amorphous TiO_2 depending on the deposition temperatures used. TiO_2 was also used to make metal oxide nanosheets using carbon nanosheets as templates. The films deposited with less then 100 cycles consisted of separated crystallites and even in the films deposited using 100 cycles pinholes could be found. By acid treatment of the carbon nanosheets it was possible to improve the nucleation, resulting in uniform and continuous films after only 50 cycles. For all processes it was found that the GPC values were lower in the pores of the AAO than on flat substrates. A lower partial pressure of the precursors inside the pores can thus be a likely cause to this observation.

In the future, it would be interesting to monitor the growth on structured substrates; this could be done using QCM, if for example carbon nanosheets were deposited on a QCM crystal. It would also be interesting to evaluate the growth of a compound in the pores of AAO using different precursors. The studies behind this work have provided some understanding of the deposition process in AAO and it would be interesting to use this knowledge to make structures for different purposes and applications. One application could be to use the AAO as a bioreactor and attach enzymes inside the pores. The enzymes could be attached to handles that are easily fixed at the pore walls. Thin films covering the pore walls could help preventing by-products such as residues of the electrolyte, incorporated in the AAO, from reaching the reaction mixture. The thin film could also improve the poor chemical inertness of the AAO, e. g., if an acidic pH is needed for the synthesis in the bioreactor.

7. Acknowledgements

First, of course, I would like to thank my supervisor Professor Anders Hårsta, whose advice, support and interest have been of great importance to me. I would also like to thank Professor Jan-Otto Carlsson for giving me the opportunity to do my Ph.D. studies at the Department of Materials Chemistry.

All the co-authors of the included papers also have my deepest gratitude; your contributions have been invaluable. In alphabetic order:

Jaan Aarik
Mats Boman
Helena Grennberg
Brian C. Holloway
Ulf Jansson
Anders Johansson
Kaupo Kukli
Erik Lindahl
Jun Lu
Ronald A. Quinlan
Erika Widenkvist

I am grateful to all the co-authors I have worked with in other projects, as well as to all my colleagues at the department and elsewhere. The technical and administrative staffs are also acknowledged.

I would also like to thank all my friends at Ångström and elsewhere who have made this time even more memorable.

Finnally, in Swedish; mamma och pappa, ett stort tack för allt. Och tack till min älskling, Erica, tack för att du finns där.

/Mårten Rooth

8. Svensk sammanfattning

Tunna filmer, ytskikt och strukturer på nanometernivå har många tillämpningar, t ex inom mikroelektronikindustrin, ytbehandling av glasögon, olika typer av sensorer och mycket annat. Med nanometernivå menas att de tunna filmerna och strukturerna har en storlek på ungefär en till något hundratal nanometer (förkortat nm). Nano är ett prefix, vilket på grekiska betyder dvärg, och en nanometer är en miljarddels meter, alltså 0,000000001 meter.

För att växa tunna filmer och strukturer har en teknik kallad ALD använts. ALD är en förkortning för engelskans *atomic layer deposition* vilket skulle kunna översättas med atomlagertillväxt. Med ALD kan man på ett mycket välkontrollerat sätt växa tunna filmer och strukturer av många olika material.

Tekniken beskrivs enklast genom ett exempel, här exemplifierat med processen för tillväxt av TiO_2. För att växa en tunnfilm av detta material med ALD används ett titaninnehållande utgångsmaterial, t ex titanjodid (TiI_4) och ett syreinnehållande utgångsmaterial t ex syrgas. Utgångsmaterialen upphettas vid behov till en temperatur då utgångsmaterialen börjar förångas, d v s materialen övergår i gasfas. Detta behöver i detta fall bara göras med titanjodiden då denna är ett fast material. Provet på vilket tunnfilmen ska växas exponeras för pulser av utgångsmaterialen i gasfas var för sig. För att skilja de olika utgångsmaterialen åt används sköljpulser med en inert gas (en gas som inte reagerar med utgångsmaterialen). Förutom att sköljpulsen separerar pulserna av utgångsmaterialen transporteras också biprodukter och överskott bort under denna puls. För varje puls av utgångsmaterialen adsorberas (fastnar) ett atomlager av utgångsmaterialet på ytan av provet. Det är bara det utgångsmaterial som har adsorberat på ytan som får möjlighet att reagera med det andra utgångsmaterialet då resten sköljs bort i den efterföljande sköljpulsen. Titanjodid som är adsorberat på ytan reagerar alltså med syre och bildar titandioxid. På det här sättet växer filmen lager för lager, därav namnet för tekniken atomlagertillväxt.

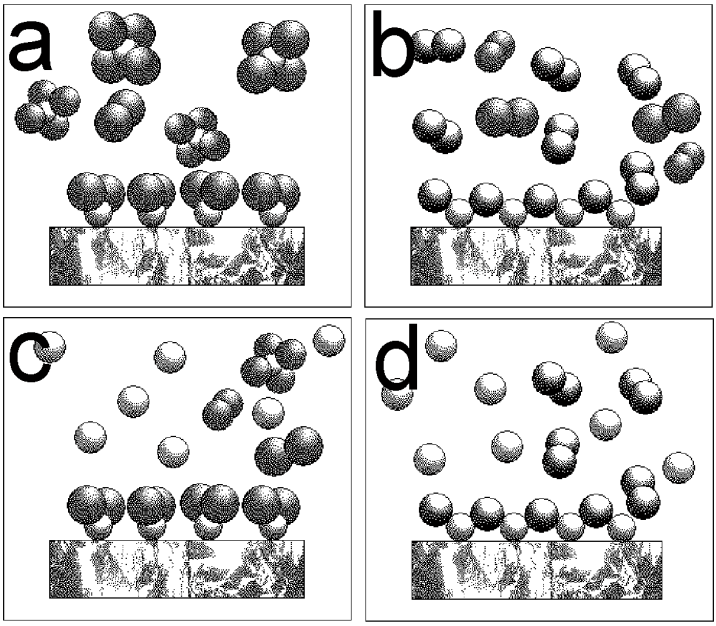

Figure 31. Schematisk beskrivning av en ALD-process för att växa TiO_2. a är titanjodidpulsen, b är den efterföljande sköljpulsen, c är syrepulsen och d är den avslutande sköljpulsen.

Då tillväxt sker med utgångsmaterial i gasfas kan prover med en komplicerad form beläggas med en jämn beläggning. Detta har använts för att göra strukturer på nanometernivå, så kallade nanostrukturer. För att tillverka nanostrukturerna måste någon form av mall (templat) användas. Som templat har i detta arbete anodisk aluminiumoxid och kolnanoflak använts (se Figur 3 och 4 i avhandlingen).

Anodisk aluminiumoxid är en porös oxid och genom att anodisera under vissa bestämda förhållanden kan porer som är parallella och ordnade i ett regelbundet mönster där varje por är omgiven av sex andra porer erhållas (se figur 3 i avhandlingen). Anodisering är en elektrokemisk process där ett material oxideras under en pålagd spänning. Porerna används sedan som templat i ALD-processen där en jämntjock tunnfilm får täcka hela strukturen. Genom att avlägsna aluminiumoxiden med hjälp av upplösning i t ex syra erhålls ett negativ av den porösa strukturen, alltså nanorör ordnade på samma sätt som porerna i den porösa aluminiumoxiden (se t ex Figur 21 i avhandlingen). Även flerväggiga nanorör tillverkades genom att växa alternerande filmer av titandioxid och järnoxid i porerna, (se t ex Figur 25 i avhandlingen).

Med kolnanoflak som templat kan metalloxidflak tillverkas med ALD, (se t ex figur 28 i avhandlingen). I detta fall etsas inte templatet bort efter att metalloxiden växts. Ytan hos kolnanoflaken är reaktionströg vilket leder till

att filmen som växer på kolnanoflaken består av öar av TiO_2 och inte en sammanhängande film. För att åstadkomma en sammanhängande film syrabehandlades proven före det att TiO_2 växtes med ALD. Syrabehandlingen bestod i att proverna lades i saltsyra vid 95 °C under sex timmar. Syrabehandlingen gav ett lyckat resultat och tunna sammanhängande filmer kunde nu växas på de syrabehandlade kolnanoflaken (se Figur 28 i avhandlingen).

9. References

1. H. S. Nalwa, *Handbook of Nanostructured Materials and Nanotechnology*, Academic Press, London, **2000**
2. G. Cao, *Nanostructures and nnaomaterials, synthesis, properties and applications*, Imperial College Press, London, **2004**
3. J. A. Venables, *Introduction to Surface and Thin Film Processes*, Cambridge University press, Cambridge, **2000**
4. Y.Y. Wu and M. Eizenberg, Mater. Chem. Phys. 2007, 101, 269
5. J. Robertson, *Eur. Phys. J.-Appl. Phys*. **2004**, 28, 265
6. T. Oyama, H. Ohsaki, Y. Tachibana, Y. Hayashi, Y. Ono, N. Horie, *Thin Solid Films* **1999**, 351, 235
7. M. Matsuoka, M. Kitano, M. Takeuchi, K. Tsujimaru, M. Anpo, J. M. Thomas, *Catal. Today* **2007**, 122, 51
8. K. Hashimoto, H. Irie, A. Fujishima, Jap. J. Appl. Phys. Part 1 **2005**, 44, 8269
9. R. L. Puurunen, *J. Appl. Phys*. **2005** 97, 121301
10. J. Lu, J. Sundqvist, M. Ottosson, A. Tarre, A. Rosental, J. Aarik, A. Hårsta, *J. Cryst. Growth* **2004**, 260, 191
11. M. Knez, K. Nielsch and L. Niinistö, *Adv. Mater* **2007**, 17, 3425
12. H. Masuda and K. Fukuda, *Science* **1995**, 268, 1466
13. J. Wollenstein, M. Burgmair, G. Plescher, T. Sulima, J. Hildenbrand, H. Bottner, I. Eisele, *Sens. Actuators, B* **2003**, 93, 442
14. E. Rios, G. Poillerat, J. F. Koenig, J. L. Gautier, P. Chartier, *Thin Solid Films* **1995** 264, 18
15. L. Mendoza, V. Albin, M. Cassir, A. Galtayries, *J. Electroanal. Chem.* **2003**, 548, 95
16. L. D. Kadam, P. S. Patil, *Sol. Energy Mater. Sol. Cells* **2001**, 70, 15
17. P. S. Patil, L. D. Kadam, C. D. Lokhande, *Sol. Energy Mater. Sol. Cells* **1998**, 53, 229
18. T. Maruyama, T. Nakai, Sol. Energy Mater. 1991, 23, 25.
19. H. K. Kim, T. Y. Seong, J. H. Lim, W. L. Cho, Y. S. Yoon, J. *Power Sources* **2001**, 102, 167
20. S. B. Ogale, R. J. Choudhary, J. P. Buban, S. E. Lofland, S. R. Shinde, S. N. Kale, V. N. Kulkarni, J. Higgins, C. Lanci, J. R. Simpson, N. D. Browning, S. Das Sarma, H. D. Drew, R. L. Greene, T. Venkatesan, *Phys. Rev. Lett*. **2003**, 91, 077 205-1

21. T. Fukumura, Y. Yamada, H. Toyosaki, T. Hasegawa, H. Koinuma, M. Kawasaki, *Appl. Surf. Sci.* **2003**, 223, 62
22. S. A. Wolf, D. D. Awschalom, R. A. Buhrman, J. M. Daughton, S. Von Molnár, M. L. Roukes, A. Y. Chtchelkanova, D. M. Treger, *Science* **2001**, 294, 1488
23. N. Özer, M. D. Rubin and C. M. Lampert, *Sol. Energy Mater. Sol. Cells* **1996**, 40, 285
24. C. M. Lampert, *Sol. Energy Mater.* **1984**, 11, 1
25. D. Rosenfeld, P. E.Schmid, S. Szeles, F. Levy, V. Demarne and A. Grisel, *Sens. Actuators B* **1996**, 37, 83
26. J. J. Van Glabbeek and R. E. Van de Leest, *Thin Solid Films* **1991**, 201, 137
27. J. Shirakashi, K. Matsumoto, N. Miura and M. Konagai, *Jpn. J. Appl. Phys.* 1997, 36, L1120
28. S. U. M. Khan and J. Akikusa, *J. Phys. Chem. B* **1999**, *103*, 7184
29. M. A. Gondal, A. Hameed, Z. H. Yamani and A. Suwaiyan, *Appl. Catal. A* **2004**, *268*, 159
30. N. Beermann, L. Vayssieres, S. -E. Lindquist, and A. Hagfeldt, *J. Electrochem. Soc.* **2000**, *147*, 2456
31. K. Siroký, J. Jireová and L. Hudec, *Thin Solid Films* **1994**, *245*, 211
32. L. Huo, Qiang Li, H. Zhao, L. Yu, S. Gao and J. Zhao, *Sens. Actuators, A* **2005**, *107*, 915
33. . C. Sun, P. C. Kuo, C. Y. Chou, S. C. Chen, C. T. Lie, M. H. Lin, J. W. Chen and H. L. Huang, *J. Magn. Magn. Mater.* **2004**, *272*, 1776
34. S. Ohta and A. Terada, *Thin Solid Films* **1986**, *143*, 73
35. Y. X. Leng, N. Huang, P. Yang, J. Y. Chen, H. Sun, J. Wang, G. J. Wan, Y. Leng, P. K. Chu, *Thin Solid Films* **2002**, 420, 408
36. M. Grätzel, *Nature*, **2001**, 414, 338
37. K.-E. Elers, M. Ritala, M. Leskelä, E. Rauhala, Appl. Surf. Sci. 1994, 82-3, 468
38. M. Schuisky, A. Hårsta, A. Aidla, K. Kukli, A.-A. Kiisler, J. Aarik, *J. Electrochem. Soc.* **2000**, 147, 3319
39. H. D. Young, R. A. Freedman, *University Physics 3rd edition*, Addison-Wesley Publishing Company **2000**
40. R. F Rolsten, *Iodide Metals and Metal Iodides*, John Wiley and sons INC., **1961**
41. H. Siimon, J. Aarik, J. *Appl. Phys. D* **1997**, 30, 1725
42. J. Sundqvist, A. Hårsta, J. Aarik, K. Kukli, A. Aidla, *Thin Solid Films* **2003**, 427, 147
43. A. P. Li, F. Müller, A. Birner, K. Nielsch and U. Gösele, *J. Appl. Phys.* **1998**, 84, 6023
44. G. E. Thompson, *Thin Solid Films* **1997**, 297, 192
45. O. Jessensky, F. Müller and U. Gösele, *J. Electrochem. Soc.* 1998, 145, 3735

46. M. Y. Zhu, J. J. Wang, B. C. Holloway, R. A. Outlaw, X. Zhao, K. Hou, V Shutthanandan and D. M. Manos, *Carbon* **2007**, 45, 2229
47. J. Wang, M. Zhu, R.A. Outlaw, X. Zhao, D.M. Manos, and B.C. Holloway, *Carbon* **2004**, 42, 2867
48. J. Wang, M.Y. Zhu, R.A. Outlaw, X. Zhao, D.M. Manos, and B.C. Holloway, *App. Phys. Lett.* **2004**, 85, 1265
49. D. B. Farmer, R. G. Gordon, *Electrochem. Solid-State Lett.* **2005**, 8, G89.
50. V. A. Coleman, R. Knut, O. Karis, H. Grennberg, U. Jansson, R. Quinlan. B. C. Holloway, B. Sanyal and O. Eriksson, *accepted for publication in J. Phys. D*
51. J. Aarik, A. Aidla, A.-A. Kiisler, T. Uustare, V. Sammelselg, *Thin Solid Films* **1999**, 340, 110
52. K. Kukli, M. Ritala, M. Leskelä and R. Lappalainen, *Chem. Vap. Deposition* **1998**, 4, 29
53. N. Hara, E. Takahashi, J. H. Yoon and K. Sugimoto, *J. Electrochem. Soc.* **1994**, 141,1669
54. K. Martin, G. McCarthy, International Center for Diffraction Data, Card 00-042-1467
55. A. Leonhardt, S. Hampel, C. Müller, I. Mönch, R. Koseva, M. Ritschel, D. Elefant, K. Biedermann and B. Büchner, *Chem. Vap. Deposition* **2006**, 12, 380
56. J. Aarik, A. Aidla, T. Uustare, K. Kukli, V. Sammelselg, M. Ritala, M. Leskelä, Appl. Surf. Sci. 2002, 193, 277
57. R. Pheamhom, C. Sunwoo, and D.-H. Kim, *J. Vac. Sci. Technol., A* **2006**, 24, 1535
58. A. Niilisk, M. Moppel, M. Pärs, I. Sildos, T. Jantson, T. Avarmaa, R. Jaaniso, J. Aarik, *Cent. Eur. J. Phys* **2006**, 4, 105
59. H. Najafov, S. Tokita, S. Ohshio, A. Kato and H. Saitoh, *Jpn. J. Appl. Phys.* **2005**, 44, 245

Acta Universitatis Upsaliensis

Digital Comprehensive Summaries of Uppsala Dissertations from the Faculty of Science and Technology 441

Editor: The Dean of the Faculty of Science and Technology

A doctoral dissertation from the Faculty of Science and Technology, Uppsala University, is usually a summary of a number of papers. A few copies of the complete dissertation are kept at major Swedish research libraries, while the summary alone is distributed internationally through the series Digital Comprehensive Summaries of Uppsala Dissertations from the Faculty of Science and Technology. (Prior to January, 2005, the series was published under the title "Comprehensive Summaries of Uppsala Dissertations from the Faculty of Science and Technology".)

Distribution: publications.uu.se
urn:nbn:se:uu:diva-0

ACTA
UNIVERSITATIS
UPSALIENSIS
UPPSALA
2008